Cite this: *Mater. Horiz.*, 2024,  
11, 3975

## From individuals to families: design and application of self-similar chiral nanomaterials

Tingting Hong,<sup>id</sup>\*<sup>a</sup> Qi Zhou,<sup>a</sup> Yilian Liu,<sup>a</sup> Jiaqi Guan,<sup>a</sup> Wenhu Zhou,<sup>id</sup><sup>bc</sup>  
Songwen Tan\*<sup>de</sup> and Zhiqiang Cai<sup>id</sup>\*<sup>ae</sup>

Establishing an intimate relationship between similar individuals is the beginning of self-extension. Various self-similar chiral nanomaterials can be designed using an individual-to-family approach, accomplishing self-extension. This self-similarity facilitates chiral communication, transmission, and amplification of synthons. We focus on describing the marriage of discrete cages to develop self-similar extended frameworks. The advantages of utilizing cage-based frameworks for chiral recognition, enantioseparation, chiral catalysis and sensing are highlighted. To further promote self-extension, fractal chiral nanomaterials with self-similar and iterated architectures have attracted tremendous attention. The beauty of a fractal family tree lies in its ability to capture the complexity and interconnectedness of a family's lineage. As a type of fractal material, nanoflowers possess an overarching importance in chiral amplification due to their large surface-to-volume ratio. This review summarizes the design and application of state-of-the-art self-similar chiral nanomaterials including cage-based extended frameworks, fractal nanomaterials, and nanoflowers. We hope this formation process from individuals to families will inherit and broaden this great chirality.

Received 26th April 2024,  
Accepted 18th June 2024

DOI: 10.1039/d4mh00496e

rsc.li/materials-horizons

### Wider impact

This review aims to be a comprehensive, authoritative, and critical review of general interest to the scientific community because of its compatible combination of knowledge from various subjects. The general trend presented in this review suggests that an individual-to-family approach is helpful in speeding up the development of self-similar chiral nanomaterials. A variety of self-similar chiral nanomaterials developed using the individual-to-family approach can realize chiral communication, transmission, and amplification. This review summarizes the design and application of state-of-the-art self-similar chiral nanomaterials including cage-based extended frameworks, fractal nanomaterials, and nanoflowers. The advantages of utilizing cage-based frameworks for chiral recognition, enantioseparation, chiral catalysis and sensing are highlighted. To further promote self-extension, fractal chiral nanomaterials with self-similar and iterated architectures have attracted tremendous attention. Nanoflowers have an overarching importance in chiral amplification due to their large surface-to-volume ratio. Since extended frameworks display their superiority over individual cages, we foresee a growing interest to various cage-based extended frameworks in chiral transmission and amplification. Considering the noteworthy merits of nano-biomaterials, we believe that much more attention should be paid to fabricating different types of biomolecule-based fractal nanomaterials. We envision that the design of self-similar nanomaterials will open up innovative avenues in chiral separation, catalysis, and sensing.

## 1. Introduction

In a self-similar world, patterns repeat themselves infinitely at different scales or levels of complexity. Herein, innovative design and application of self-similar chiral nanomaterials

are shared. If an intimate relationship is established between similar individuals, self-extension begins. The marriage of similar chiral synthons facilitates the inheriting and broadening of chirality. A fractal family tree represents the further self-extension of iterated chiral architectures. We envision that this individual-to-family approach will preserve the chirality of self-similar nanomaterials forever.

Chirality is considered a ubiquitous attribute for the sustainability of life in nature. Chiral substances with pure enantiomeric forms play a significant role in the generation and evolution of life.<sup>1–3</sup> Developing innovative nanomaterials has occupied a crucial position in enantioseparation, chiral catalysis and sensing research.<sup>4–11</sup> How to realize chiral communication, transmission,

<sup>a</sup> School of Pharmacy, Changzhou University, Changzhou, Jiangsu 213164, China.  
E-mail: zhqcai@cczu.edu.cn, hongtingting0203@163.com

<sup>b</sup> Xiangya School of Pharmaceutical Sciences, Central South University, 172  
Tongzipo Road, Changsha, Hunan 410013, China

<sup>c</sup> Academician Workstation, Changsha Medical University, Changsha 410219, China

<sup>d</sup> Monash Suzhou Research Institute, Monash University, Suzhou SIP 215000,  
China. E-mail: songwen.tan@monash.edu

<sup>e</sup> Jiangsu Dawning Pharmaceutical Co., Ltd., Changzhou, Jiangsu 213100, China

and amplification of chiral units? Self-similar nanomaterials can be designed using a bottom-up process from individuals to

families, achieving self-extension. We have summarized the cooperation between nanomaterials and biomolecules in chiral



**Tingting Hong**

*Tingting Hong obtained her PhD degree from China Pharmaceutical University in 2017. During 2016–2017, she worked as a CSC joint-PhD student in Vrije Universiteit Brussel. During 2018–2020, she was a postdoc undergoing research mainly focused on chiral separation science at Central South University. She is currently a teacher at Changzhou University. She has published several papers on chiral separation, nanomaterials, and capillary electrophoresis in Analytical chemistry, Microchimica Acta, Nanoscale Horizons, Journal of Chromatography A, Talanta, Analytica chimica acta, Analyst, Anal Bioanal Chem, Electrophoresis, Journal of Separation Science, Analytical Biochemistry and Trends in Analytical Chemistry.*

*Journal of Chromatography A, Talanta, Analytica chimica acta, Analyst, Anal Bioanal Chem, Electrophoresis, Journal of Separation Science, Analytical Biochemistry and Trends in Analytical Chemistry.*



**Qi Zhou**

*Qi Zhou is currently a postgraduate student in Changzhou University and majors in chiral separation. His research focuses on the preparation of nanomaterial-modified capillary monoliths for separation science and biomolecules immobilization in microscale systems.*



**Yilian Liu**

*Yilian Liu is currently a postgraduate student in Changzhou University and majors in chiral separation. Her research interests include fabrication of nanoflower-based microscale systems and application of microscale systems for enantioseparation.*



**Jiaqi Guan**

*Jiaqi Guan is currently a postgraduate student in Changzhou University and majors in chiral separation. His research focuses on preparation of nanomaterial-modified capillary monoliths for chiral separation and nanoflower immobilization in microscale systems.*



**Wenhui Zhou**

*Wenhui Zhou obtained his PhD degree from Central South University in 2016. From 2014 to 2016, he worked as a CSC joint-PhD student at the University of Waterloo. He is currently a professor at Central South University. He has published several papers about nanomaterials, functional nucleic acids, bioanalysis, capillary electrophoresis, biomedicine, pharmaceuticals, and cancer therapy in Nanoscale, Analytical chemistry, Analyst, Nano Letters, ACS Applied Materials & Interfaces, Acta Biomaterialia, Microchimica Acta, Analytica Chimica Acta, and so forth.*

*ACS Applied Materials & Interfaces, Acta Biomaterialia, Microchimica Acta, Analytica Chimica Acta, and so forth.*



**Songwen Tan**

*Songwen Tan obtained his PhD degree from University of Sydney in 2019. From 2019 to 2023, he worked as a professor at Central South University. He is currently working at Monash University. He has published several papers on nanomaterials, capillary electrophoresis, bioanalysis, pharmaceuticals, environment and food analysis in Analytical chemistry, Analyst, Talanta, Trends Food Sci Technol, Food Hydrocoll, Chemosphere, Powder Technology, Materials & Design, Energy, Environmental Toxicology and Pharmacology, Bioresource Technology, Biotechnology Letters, and so forth.*

*Materials & Design, Energy, Environmental Toxicology and Pharmacology, Bioresource Technology, Biotechnology Letters, and so forth.*

sensing and separation.<sup>12</sup> In the present review, we further describe recent developments in periodic nanostructures from the point of view of chirality applications.

The marriage of cages facilitates the construction of various self-similar extended frameworks. Cage compounds are polycyclic compounds possessing the shape of a cage.<sup>13–15</sup> Transformation of discrete cages into extended frameworks gives them much more complexity and multifunctionality. The cage-to-framework strategy provides an avenue for inheriting and broadening the chirality of the cages. Porous organic cages (POCs) have emerged as ‘rising stars’ of nanomaterials that stand out by merit of their modularity, tunability, and processability.<sup>16–19</sup> Based on their unique features, POCs provide an alternative approach to molecular recognition, gas storage, and catalysis reaction. Though substantial achievements have been made, there are avenues still worth investigating to expand novel application scenarios. Chiral self-sorting is the high-fidelity recognition of self from non-self within racemates.<sup>20</sup> Chiral self-sorting of POCs has rapidly gained popularity. Metal–organic cages (MOCs) are discrete entities composing metal moieties and organic bridging linkers.<sup>21–23</sup> Innovative ‘cage-in-cage’ frameworks based on MOCs exhibit desirable chiral separation abilities. Different types of chiral extended frameworks including metal–organic frameworks (MOFs), hydrogen-bonded organic frameworks (HOFs), polymers, and polycatenanes can be generated by choosing cages as building blocks.<sup>24</sup> Due to their specific advantages, cage-based frameworks have been widely applied for chiral recognition, chiral catalysis and sensing, enantioseparation, and chiral optics. This cage-to-framework approach is able to achieve the communication, transmission, and amplification of chirality.

A fractal refers to infinitely self-similar and iterated mathematical constructs.<sup>25–27</sup> Fractal-like patterns such as trees, flowers, snowflakes, coastlines, and blood vessel branching are prevalent in nature, displaying the beauty of the real world. The combination of fractal geometry and chirality can expand human cognition boundaries.<sup>28,29</sup> In the context of nanomaterials, these self-similar architectures possess smaller components resembling the overall structure. Fractal nanomaterials are considered a desirable alternative for chirality transmission due to their intricate and highly interconnected structure. When applied to

flowers, fractals can capture the arrangement of petals.<sup>30,31</sup> A variety of macroscopic flowers including peony, chrysanthemum, rose, and dandelion possess chirality in asymmetric floral structures. The design of state-of-the-art chiral nanoflowers with self-similarity has received considerable interest. Chiral nanoflowers provide favourable alternatives for developing chiroptical materials. Tremendous endeavors are focused on constructing nanoflower-based circularly polarized luminescence (CPL) materials with chiroptical activity. Chiral transmission and amplification benefit from the attractive advantages of nanoflowers including their large surface-to-volume ratio and high stability.

We showcase the design and application of various self-similar chiral nanomaterials. Scientists’ novel ideas have made tremendous contributions to chiral separation, enantioselective recognition, chiral catalysis and sensing. Self-similar materials can be formed using a bottom-up process from individuals to families, realizing self-extension. This fabrication strategy is helpful in promoting the communication, transmission and amplification of chirality. We will describe the marriage of cage building blocks to construct multifarious extended frameworks including MOFs, HOFs, polymers, and polycatenanes. The self-sorting of POCs for developing chiral architectures will be highlighted. Moreover, a state-of-the-art cage-in-cage framework can be synthesized based on porous coordination cages (PCCs). Attributing to the self-similar properties of a fractal, fractal nanomaterials are considered desirable alternatives for chirality transmission. We will review advances in different types of fractal nanomaterials utilized for chiral applications. The prospect of using specific features of fractal chirality for designing hierarchical chiral materials will be further summarized. Flower-like patterns that exhibit self-similarity can be created by using mathematical algorithms inspired by fractals. The advantages of applying nanoflowers in the development of chiroptical materials will be described. A variety of enzyme-based NFs have been used for chiral catalysis. We envision that the design of self-similar nanomaterials will open up innovative avenues in chiral separation, catalysis, and sensing.

## 2. Marriage of chiral cages

The marriage of cages provides state-of-the-art opportunities for developing favourable chiral materials. The application of cages as units for the high-order assembly into extended frameworks has introduced complexity and diversity to the resulting structures. Chiral self-sorting of cages is a desirable strategy to construct chiral architectures. Increasing attention has been paid to the self-sorting of POCs for fabricating structures with a satisfactory chiral recognition capability. Different types of chiral extended frameworks including MOFs, HOFs, polymers, and polycatenanes have been synthesized by selecting cages as building blocks. In addition, the design of new cage-in-cage frameworks is described in this section. Noteworthy efforts have been made to realize chiral transmission and amplification by utilizing the cage-to-framework strategy. Moreover, chirality communication in interpenetrated architectures is also discussed. The advantages of applying innovative



Zhiqiang Cai

*Zhiqiang Cai obtained his PhD degree from Zhejiang University. Zhiqiang Cai is currently a professor at the school of pharmacy in Changzhou University. Professor Cai's research interests include biotechnology, biocatalysis, capillary electrophoresis, nanomaterials, and fermentation engineering with several publications in Analytical Chemistry, Nanomaterials, Biosensors and Bioelectronics, Analyst, Journal of Agricultural and Food Chemistry and so forth.*

cage-based frameworks for chiral recognition, enantioseparation, chiral catalysis and sensing are highlighted in this review.

## 2.1 From porous organic cages to extended frameworks

POCs have been widely utilized in different fields such as gas storage, sensing, catalysis, and enantioseparation.<sup>32–37</sup> As a type of porous material, POCs are assembled by discrete, cage-like molecules with intrinsic and guest-accessible cavities *via* weak intermolecular forces.<sup>38–41</sup> Compared with extended porous frameworks generated by chemical bonds, POCs exhibit desirable solubility in common organic solvents. In addition, POCs specific structure property facilitates the investigation of chiral self-sorting from covalent to weak non-covalent bonds. Self-sorting is a complicated phenomenon that commonly exists in biological systems. Chiral self-sorting is the high-fidelity recognition of self from non-self within racemates. Chiral self-sorting of POCs has attracted tremendous attention.<sup>42–44</sup> Chiral octahedral aromatic cages including PAC 1-*S* and 1-*R* were prepared by condensation of 2,4,6-triformylphloroglucinol and binaphthylenediamine. Results indicated that the chiral narcissistic and self-sorting on the supramolecular assembly of racemic cages were able to be regulated by  $\pi$ - $\pi$  and C-H... $\pi$  interactions. The racemic structure (1-*R/S*) was formed

based on the stacking of two enantiomer cages in wall-to-wall patterns when choosing mesitylene as the solvent (Fig. 1(a) and (b)). These racemic co-crystals were able to return to homochiral crystallization in toluene. Therefore, the homochiral and racemic crystallization displayed supramolecular structural reversible transformations. Furthermore, the proposed homochiral structure exhibited a desirable enantioselectivity toward axially chiral aromatic molecules.

Homochiral porous materials including MOFs, covalent-organic frameworks (COFs), POCs and MOCs with high surface area, various chemical functionality and adjustable topology have been widely applied for chiral recognition, asymmetric catalysis, and chiral separation.<sup>45–51</sup> For instance, two homochiral POCs, CPOC-401-Pro and CPOC-302-Pro, were constructed depending on a supramolecular tetraformyl-resorcin[4]arene scaffold with distinct chiral proline-functionalized diamine ligands.<sup>52</sup> The anchored chiral proline catalytic centers and the inherent confined cavities enabled the POCs to catalyze asymmetric aldol reactions with desirable catalytic performance. To develop a high performance liquid chromatography (HPLC) chiral stationary phase, a chiral POC, NC1-*R* was immobilized onto thiol-modified silica based on a click reaction.<sup>53</sup> The proposed

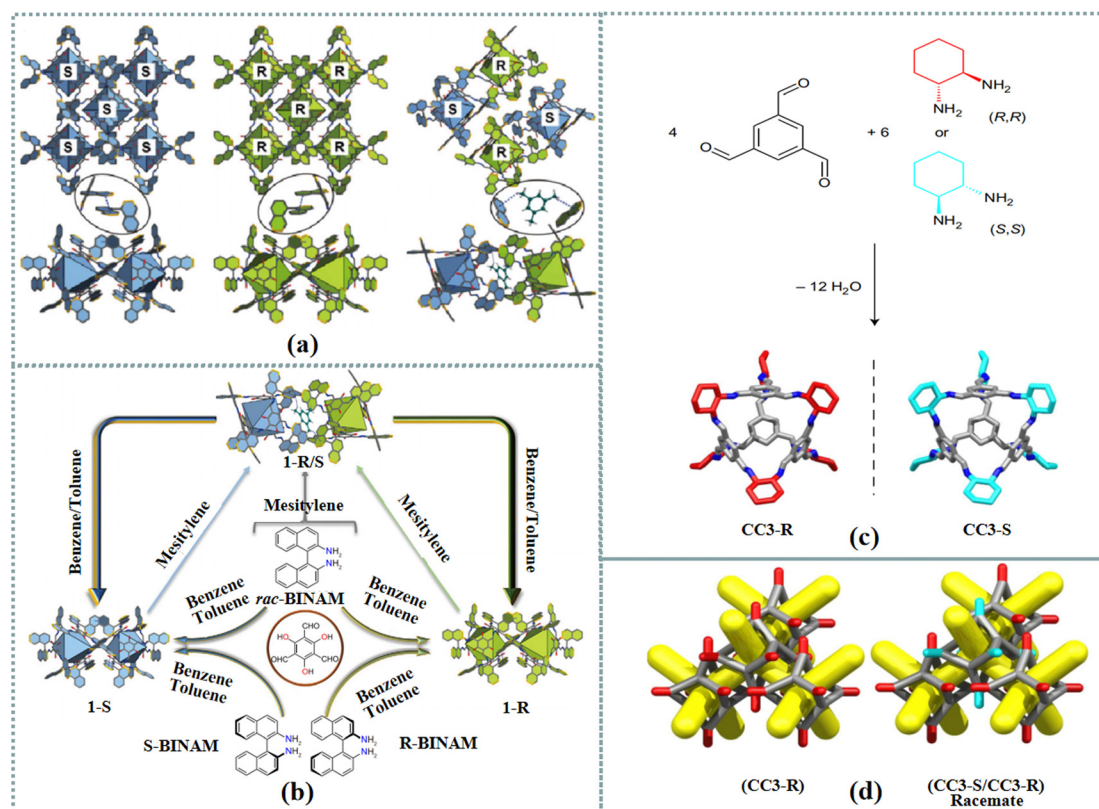


**Fig. 1** (a) Schematic representation of the interaction between cages and between solvent molecules and cages in homochiral and heterochiral structures. (b) Schematic illustration of the structural formation. The synthesis of cages 1 and the reversible supramolecular structural transformation between homochiral and racemic structures under different solvents.<sup>42</sup> Reproduced with permission from ref. 42. Copyright 2022 Springer Nature. (c) Synthesis of porous tetrahedral cages **CC3-R** and **CC3-S** from triformylbenzene (TFB) and CHDA. For **CC3-R**, the cyclohexane groups are shown in red and for **CC3-S** they are shown in turquoise; other C, grey; N, blue; H, omitted. (d) Schematic representation of the desolvated homochiral **CC3-R** and racemic (**CC3-R/CC3-S**) crystal structures; the pore network is shown in yellow, simplified cage frame in grey and simplified cyclohexyl vertices in red (R) and turquoise (S).<sup>56</sup> Reproduced with permission from ref. 56. Copyright 2017 Springer Nature.

stationary phase involving a cationic imidazolium spacer presented satisfactory chiral separation ability for various enantiomers. A hydroxyl-modified homochiral POC-1 was prepared *via* the one-step [4+6] condensation of (1*R*,2*R*)-diphenylethylenediamine with 2-hydroxy-1,3,5-triformylbenzene.<sup>54</sup> Furthermore, the POC was utilized as the stationary phase to develop a capillary gas chromatography column. The resulting column presented favourable separation performance for a variety of racemates such as alcohols, diols, halohydrocarbons, epoxides, *etc.* A molecular organic cage was utilized to separate an aromatic feedstock (mesitylene) from its structural isomer (4-ethyltoluene) with desirable specificity.<sup>55</sup> Though POCs presented better solubility in the solvent, the structures and functions of POCs are less diverse than those of MOFs and COFs. POCs can be employed as macromolecular ligands and coordinated with metal ions to synthesize MOFs, creating novel perspectives for generating extrinsic cage porosity. HOFs were able to be formed by supramolecular assembly of POCs *via* hydrogen-bonding interactions. As an innovative chiral porous material with the properties of a chiral pore environment and multiple spatial topological architecture, chiral frameworks display enormous potential in chiral applications. Efforts have been devoted to developing extended frameworks based on POCs for chiral applications. Cooper *et al.* prepared 1D porous nanotubes and 3D diamondoid pillared porous networks based on tubular covalent cages.<sup>56</sup> The chiral cage CC3-S possessed four windows positioned in a tetrahedral arrangement (Fig. 1(c) and (d)). Due to heterochiral window-to-window interactions with CC3-R, CCS-S packed more closely to CC3-R than its homochiral equivalents. These tetrahedral cages were able to produce 3D pore networks. Two isorecticular porous pillared structures were developed by heterochiral co-crystallization of tubular and tetrahedral chiral building blocks. The resulting networks were analogous to extended frameworks composed of linear ditopic organic linkers and tetrahedral metal nodes. The CC2 cage's chirality played an important role in affecting its tendency to catenate because homochiral catenanes were formed.<sup>57</sup> This phenomenon was attributed to the fact that cages 'self-sort' to create catenanes comprising two cages with the same chirality. Moreover, chiral interconversion was realized in solution for CC1 and CC13.

Self-sorting of POCs provides a promising strategy for developing efficient enantioselective materials. The superiority of extended frameworks over individual chiral cages has been discussed. Studies indicate that POCs can be considered satisfactory units for the construction of desirable chiral architectures.

## 2.2 From metal-organic cages to extended frameworks

MOCs are discrete, supramolecular entities composed of metal moieties and organic bridging linkers.<sup>58–60</sup> To some extent, MOCs can be considered as secondary building units of MOFs since MOCs and MOFs possess similar components and assembly principles. Nevertheless, MOCs with discrete structures display different properties from MOFs in terms of solubility, topology, dimension, and stability. MOCs have gained tremendous interest in catalysis, biomedical science, and molecular separation.<sup>61–69</sup> High-dimensional materials such as MOFs, HOFs, and polymers

are able to be hierarchically synthesized by choosing MOCs as building blocks. Many efforts have been focused on exploring 'cage-based extended frameworks'. The incorporation of chirality into the design of MOCs enables these supramolecules to possess specific potentials in enantioselective separation, chiral amplification, and chiroptical application.

As a type of MOCs, PCCs possess well-defined nanosized cavities. The preparation of discrete nanoscale MOCs with specific configurations and cavities has attracted tremendous interest in material science.<sup>70–74</sup> A homochiral PCC, ( $\Delta/\Lambda$ )<sub>12</sub>-PCC-57, was prepared based on the reaction between carboxyl-modified amino acid and lanthanum cations.<sup>75</sup> The resulting dodecanuclear lanthanide cage possessed an octahedral 'cage-in-cage' framework. As seen in Fig. 2, one inner octahedral cage is embedded by a second outer octahedral cage. The inner and outer shells comprised four L-ligands, sharing six La<sub>2</sub> clusters on the octahedron apices. Two distinct geometries including 'fold' and 'stretch' configurations were obtained due to steric hindrance around the octahedron vertex and the high flexibility of L-ligand. The inner cage was formed based on the 'stretch' configuration of L-ligands, whereas the outer cage was formed depending on the 'fold' configuration. During the self-assembly process, the chirality was transferred from the ligand to La(III) centers. All 12 metal centers were endowed with homochiral stereochemistry. Therefore, the proposed ( $\Delta/\Lambda$ )<sub>12</sub>-PCC-57 possessed a multi-chiral microenvironment. The chiral cavity in PCC-57 was decorated with diverse hydrophilic amide groups pointing inward, providing a desirable platform for exploring the interactions between the cage and enantiomers. Efficient chiral separation of various organic molecules and drug intermediates was achieved.

Two porous assemblies, PCC-60 and PCC-67, were developed by using isostructural lanthanide octahedral cages.<sup>76</sup> The PCC-67 applied a densely packed mode, while the PCC-60 was a hierarchically porous assembly containing interconnected mesopores. A spindle-like mesopore was able to be formed based on the orderly arrangement of 12 octahedral cages (Fig. 3(a)–(e)). Since the coordination cage's open windows were oriented toward the extrinsic mesopore, the formed interconnected channels were beneficial to the mass transfer within the PCC-60 superstructure. Results indicated that the hierarchical pores existing in PCC-60 enabled shortening of the equilibrium time for adsorbing chiral analytes. The PCC-60 presented a desirable chiral separation ability toward racemic diols and amides. Furthermore, the resulting PCC-60 was used as a chiral stationary phase for HPLC, and baseline separation of six pharmaceutical intermediates was achieved. Compared with the PCC-67 with uniform microporous cavities, PCC-60 presented higher enantiomeric excess values in separating enantiomers. An anionic Ti<sub>4</sub>L<sub>6</sub> (L = embonate) cage was extended and fixed into a homochiral microporous framework (PTC-236( $\Delta$ ) or PTC-236( $\Lambda$ )) *via* a post-assembly modification approach to improve its stability in the crystal state.<sup>77</sup> The microporous framework of PTC-236 was prepared by using  $\Delta\Delta\Delta\Delta$ - or  $\Lambda\Lambda\Lambda\Lambda$ -[Ti<sub>4</sub>L<sub>6</sub>] cages with triple-stranded right- or left-handed helical Zn-bimbo chains (Fig. 3(f)–(h)). Although a few cages were able to be organized into networks *via* other methods, these

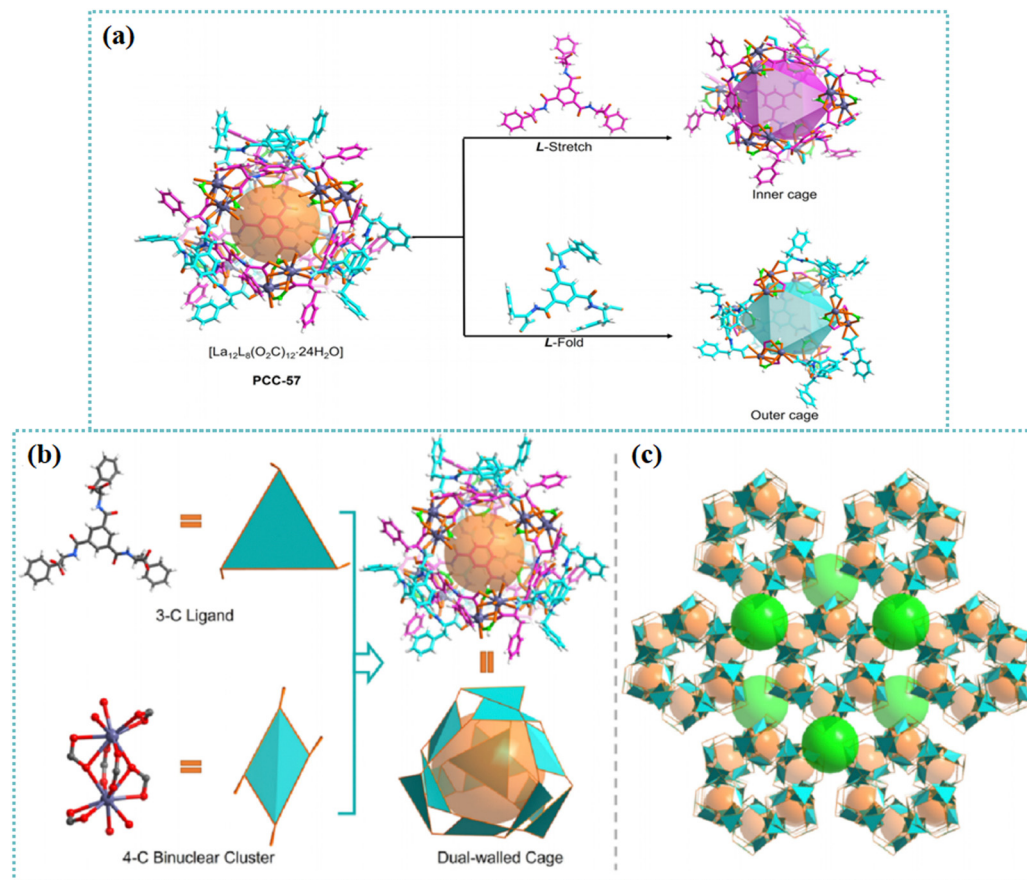
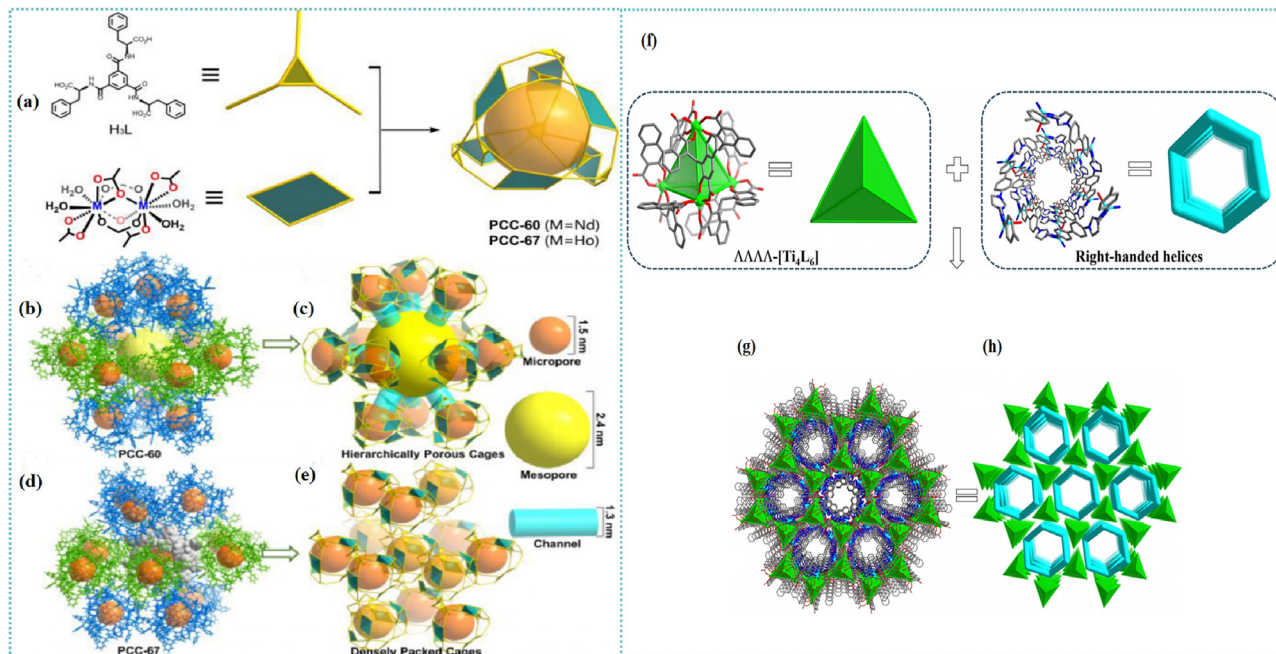


Fig. 2 (a) View of the structures of the dual-walled coordination cage and its octahedral inner (purple) and outer (cyan) cage assembled by the flexible ligand and lanthanum ion. (b) Illustration of the connectivity of the bridging ligand and binuclear metal node in the dual-walled PCC-57. (c) View of the packing mode of the dual-walled cage (highlighted as the yellow ball) along the *c*-axis and the large cavity (highlighted as the green ball) formed via the orderly arrangement of PCC-57.<sup>75</sup> Reproduced with permission from ref. 75. Copyright 2021 American Chemical Society.

transformed complexes possessed poor structural stability and crystallinity. The resulting PTC-236 was highly stable in different types of solvents. Moreover, PTC-236 was able to be used for recognizing and separating isomeric molecules. Two homochiral frameworks (PTC-108( $\Delta$ ) and PTC-108( $\Lambda$ )) with supramolecular architectures were synthesized based on  $[\text{Ti}_4\text{L}_6]$  cages.<sup>78</sup> The cage displayed a desirable enantioselective recognition ability toward chiral organic and pharmaceutical molecules. Chiral transference and amplification were realized from an enantiopure molecule to homochiral framework. The racemic tetrahedral  $[\text{Ti}_4\text{L}_6]^{8-}$  cages ( $\text{L}$  = pamoic acid) were resolved into their  $\Delta\Delta\Delta\Delta$  and  $\Lambda\Lambda\Lambda\Lambda$  enantiomers by enantiopure left- and right-handed  $[\text{Ag}_4(\text{R}/\text{S}-\text{L}_1)_5]^{4+}$  ( $\text{L}_1$  = 1*R*/2*S*,2*R*/*S*(-)-1,2-diaminocyclohexane) cations, respectively.<sup>79</sup> A 3D superstructure was obtained based on the connectivity between  $[\text{Ag}_4(\text{R}/\text{S}-\text{L}_1)_5]^{4+}$  and  $[\text{Ag}(\text{H}_2\text{O})_3]^+$  cations with  $[\text{Ti}_4\text{L}_6]$  anionic cages. Furthermore, 10  $\Lambda\Lambda\Lambda\Lambda$ - $[\text{Ti}_4\text{L}_6]$  cages and 3  $[\text{Ag}(\text{H}_2\text{O})_3]^+$  units as well as 9  $[\text{Ag}_4(\text{R}/\text{S}-\text{L}_1)_5]^{4+}$  units were applied for constructing a larger diamondoid cage. Two homochiral supramolecular compounds (PTC-232( $\Delta$ ) and PTC-232( $\Lambda$ )) with interpenetrating dia-type frameworks were able to be formed (Fig. 4). To avoid the aggregation-caused quenching effect and amplify the CPL activities, planar-chiral [2.2]paracyclophane (pCp) chromophores were reticulated into stable Zr(IV) MOFs.<sup>80</sup>

Octahedral cages were formed based on six hexanuclear clusters and eight  $\text{L}^1$  linkers. One cage was surrounded by eight adjacent cages by sharing faces to generate a 3D porous network with interconnecting 1D channels (Fig. 5). The  $\text{Zr}_6$  cluster in pCp-2 was different from pCp-1. The neighboring  $\text{Zr}_6$  clusters along the *c* direction were connected depending on four ligands to create a cage. The cage extended in three directions producing a network possessing triangular channels. Compared with the free pCp linkers, the incorporation of chiral pCp into crystalline Zr-MOFs was able to amplify the dissymmetry factor and improve luminescence efficiency. This work provided an efficient method to develop chiroptical materials. The cationic cage  $[\{\text{Cu}_6(\text{H}_2\text{O})_{12}\}\{\text{TPTA}\}_8]^{12+}$  (TPTA = tris(3-pyridylamino)thiophosphate) was assembled into 1D, 2D and 3D MOFs by sequentially replacing Cu-bound aqua ligands in the chiral cage with connecting chloride ions.<sup>81</sup> These networks were able to be disassembled into lower dimensional frameworks by utilizing  $\text{AgNO}_3$  or  $(n\text{Bu}_4\text{N})\text{NO}_3$ . This work provided an efficient strategy for the reversible synthesis of cage-connected networks. Homochiral MOFs  $\text{Cu}_3(\text{bipy})_3((\text{S})\text{-TMTA})_2(\text{H}_2\text{O})_4$  were synthesized by the self-assembly of  $\text{Cu}(\text{NO}_3)_2 \cdot 3\text{H}_2\text{O}$  and (*S/R*)- $\text{H}_3\text{TMTA}$  in the presence of 4,4'-bipyridine (bipy) linker.<sup>82</sup> The chiral ligands connected by the hydrogen bonds were arranged in a right/left-handed helix. The chirality was able to be transferred



**Fig. 3** (a) Construction of the octahedral cages of PCC-60 and PCC-67. Views of (b) the arrangement of octahedral cages and (c) the hierarchical porous structure in the supramolecular assembly of PCC-60; views of (d) the densely packed mode of octahedral cages and (e) microporous structure in PCC-67. The orange ball represents the inner cavity, while the yellow ball represents the large external cavity. The gray molecule represents a single octahedral cage surrounded by 12 cages.<sup>76</sup> Reproduced with permission from ref. 76. Copyright 2022 American Chemical Society. (f) Crystal structures of  $\Lambda\Lambda\Lambda\Lambda$ -[Ti<sub>4</sub>L<sub>6</sub>] and the triple-stranded right-handed helical chains along the *c*-axis formed by 4,4'-di(1*H*-imidazol-1-yl)-1,1'-biphenyl (bimb) ligands and Zn<sup>II</sup>. (g) and (h) 3D framework and simplified structure with helical chiral channels.<sup>77</sup> Reproduced with permission from ref. 77. Copyright 2023 John Wiley and Sons.

from the chiral carbon atoms to the helices based on hydrogen bonds. An extended three-dimensional structure was formed due to the stacking of these chains. A homochiral MOF with an expanded open cage based on (*R*)-3,3'-bis(6-carboxy-2-naphthyl)-2,2'-dihydroxy-1,1'-binaphthyl ligand was prepared for developing the HPLC chiral stationary phase.<sup>83</sup> The resulting column presented a desirable chiral separation ability. An extended 3D framework was obtained by combining cage complexes isolated and functionalized prior to preparation.<sup>84</sup> Multiple Lewis base modified sites were introduced to the periphery of a pre-prepared cage. This functionalized cage was able to bind to other cages with Lewis acidic sites. As a bidentate linker, a [Pr<sub>2</sub>NH<sub>2</sub>][Cr<sub>7</sub>NiF<sub>8</sub>(O<sub>2</sub>C<sup>t</sup>Bu)<sub>14</sub>(O<sub>2</sub>CC<sub>5</sub>H<sub>4</sub>N)<sub>2</sub>] chiral molecule was bridged between three nodes of the [Fe<sub>2</sub>CoO(O<sub>2</sub>C<sup>t</sup>Bu)<sub>6</sub>(HO<sub>2</sub>C<sup>t</sup>Bu)<sub>3</sub>] cage. This work provided an efficient strategy to develop an extended framework without adding organic linker or serendipitously assembling cages *in situ*. In addition to MOFs, HOFs were constructed based on non-covalent bonds.<sup>85</sup> The HOF's structure consisted of organic molecules connected by hydrogen bond moieties. The intermolecular interactions between the cages facilitated the improvement in structural stability. Stable cubic cage-based HOFs were fabricated *via* multiple charge-assisted hydrogen bonds between coordination cages and chloride ions. Liu *et al.* utilized chiral porous hydrogen bonded frameworks with Brønsted acid groups for recyclable heterogeneous asymmetric catalysis.<sup>86</sup> The hierarchical assembly of the cages was achieved by intercage hydrogen-bonds and hydrophobic interactions. The results indicated that the HOF catalyst was able to be recovered and recycled at least ten times with desirable

activity and enantioselectivity. This work paved the way for developing innovative metallocage-based porous materials in chiral sensing, optics, catalysis, recognition and separation.

The cage-to-framework approach facilitates the construction of hybrid materials with various functionalities. Porous MOFs were able to be developed by linking MOCs with ligands to generate infinite sustained architectures. Cage-based HOFs were formed depending on hydrogen bond moieties. The cage-to-framework strategy was also utilized to develop polymers by choosing POCs as chiral synthons. This strategy facilitated the improvement in POCs internal cavity accessibility and generation of porous materials possessing both intrinsic and extrinsic cage porosity. A 2D double-layered dibenzoyl-tartrate chiral coordination polymer was formed based on [Mn<sub>4</sub>L<sub>2</sub>(bpp)<sub>4</sub>] tetrahedral cages linked by dibenzoyl-tartrate spacers.<sup>87</sup> Su *et al.* developed chiral lanthanide coordination polymers with channels formed by inter-connecting 16 lanthanide-based cage-like building units.<sup>88</sup>

The cage-to-framework strategy realized the conversion of cages to MOFs, HOFs, and polymers. Cages were considered favourable building blocks to fabricate hierarchically porous materials. This cage-to-framework approach facilitated the enhancement of a cage's surface area by forming extrinsic porosity. Additionally, the cage-based frameworks inherited the original characteristics of cages, representing an innovative generation of advanced chiral porous materials. The advantages of applying 'cage-in-cage' frameworks for chiral separation are discussed in this section. Moreover, MOC-based extended frameworks are considered desirable HPLC chiral stationary phases.

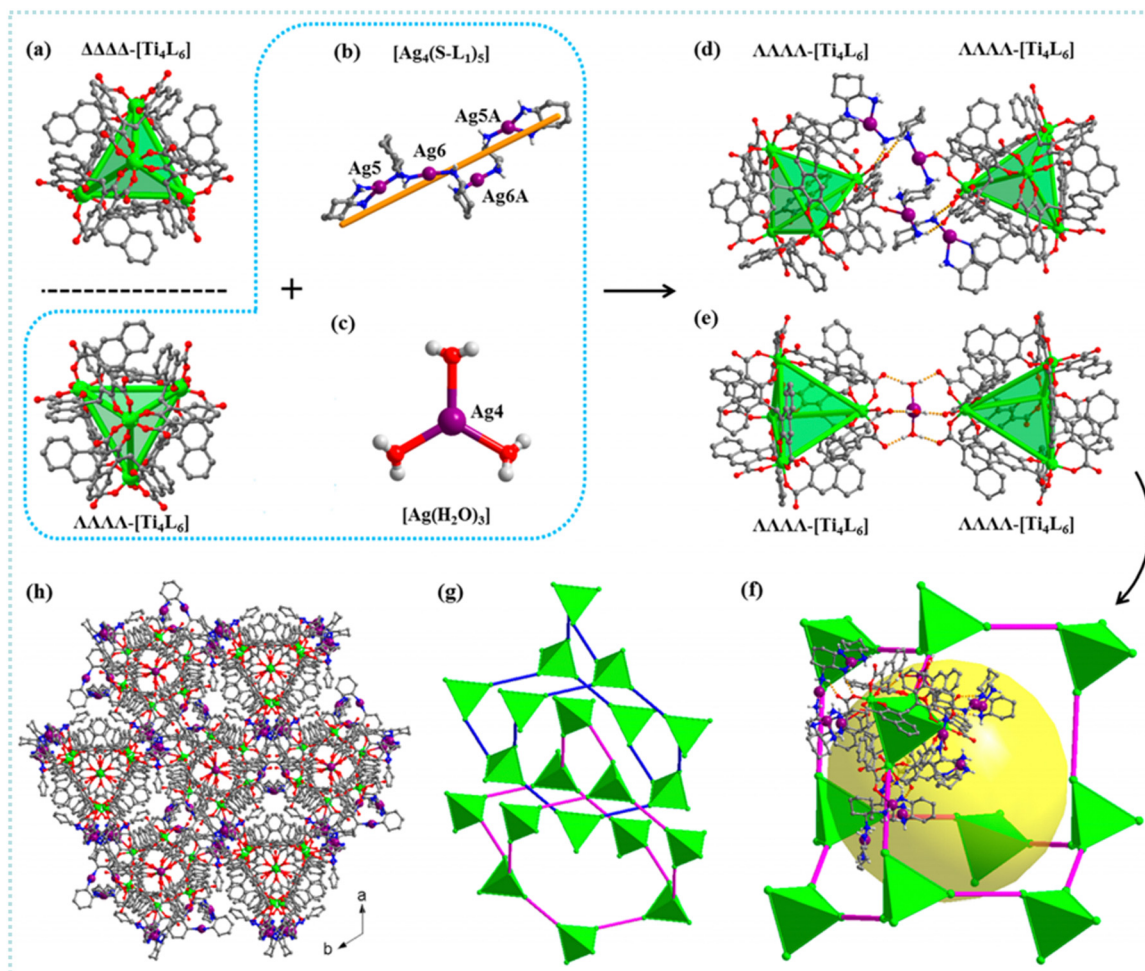


**Fig. 4** (a) The crystal structures of the enantiomers:  $\Delta\Delta\Delta\Delta$ -[Ti<sub>4</sub>L<sub>6</sub>] (top) and  $\Lambda\Lambda\Lambda\Lambda$ -[Ti<sub>4</sub>L<sub>6</sub>] (bottom); (b) and (c) the [Ag<sub>4</sub>(S-L<sub>1</sub>)<sub>5</sub>]<sup>4+</sup> and [Ag(H<sub>2</sub>O)<sub>3</sub>]<sup>+</sup> ions in PTC-232(Δ,S); (d) and (e) two neighboring  $\Lambda\Lambda\Lambda\Lambda$ -[Ti<sub>4</sub>L<sub>6</sub>] cages connected by one [Ag<sub>4</sub>(S-L<sub>1</sub>)<sub>5</sub>]<sup>4+</sup> and one [Ag(H<sub>2</sub>O)<sub>3</sub>]<sup>+</sup> unit through coordination bonds and hydrogen bonds, respectively; (f) the diamondoid cage constructed by  $\Lambda\Lambda\Lambda\Lambda$ -[Ti<sub>4</sub>L<sub>6</sub>] cages and [Ag<sub>4</sub>(S-L<sub>1</sub>)<sub>5</sub>]<sup>4+</sup> and [Ag(H<sub>2</sub>O)<sub>3</sub>]<sup>+</sup> units in PTC-232(Δ,S); (g) 2-fold interpenetrating dia-type topology; (h) the 3D packing structure of PTC-232(Δ,S). Atom color code: green, Ti; purple, Ag; red, O; blue, N; gray, C.<sup>79</sup> Reproduced with permission from ref. 79. Copyright 2020 American Chemical Society.

Substantial advances have been made in utilizing different types of MOC-based frameworks for enantioseparation, chiral amplification, and asymmetric catalysis.

### 2.3 From metal-organic cages to polycatenanes

The ‘mechanical bond’ was described by Nobel laureates J. Fraser Stoddart and Carson J. Bruns in their famous work ‘The Nature of the Mechanical Bond: From Molecules to Machines’.<sup>89,90</sup> As the paramount physical bond, a mechanical bond is formed between subcomponents of a compound. The chemistry of the mechanical bond is utilized for designing and generating catenanes, rotaxanes, molecular shuttles, and artificial molecular machines. Catenanes, consisting of *n* consecutively interlocking rings, are a type of mechanically interlocked molecules. Polycatenane is a mechanically linked polymer stemmed from catenane subunits.<sup>91–93</sup> The exploration of catenanes prompted the development of artificial molecular machines in supramolecular chemistry. Moreover, catenanes have attracted increasing attention for their topological chirality.

Chirality communication at a molecular and supramolecular level is the elementary property enabling the individual chiral elements to employ coincident chiral conformations and brings about the accumulation and amplification of the overall chiral sense. A variety of traditional approaches were investigated to huddle the individuals together for communication.<sup>94–97</sup> To avoid the disadvantages of the one-step chirality communication mode, Gan *et al.* explored three sequential steps to manipulate communication of aromatic oligoamide sequences within the interpenetrated helicate structure.<sup>98</sup> This architecture facilitated the accumulation and transmission of chiral information on the side chains to the sequence’s helical backbones. The chirality of aromatic amide sequences derived from the amide segment’s twisting feature, led to the P or M helical conformation of the molecular strands. Four isomers (PPPP/MMMM and PMMP/MPPM) of the interpenetrated helicates were formed due to the communication between the ligands (Fig. 6(A)). Furthermore, a contraction state (PPPP and MMMM) was obtained by encapsulating Cl<sup>−</sup> anions with the dimeric helicate. The reversible

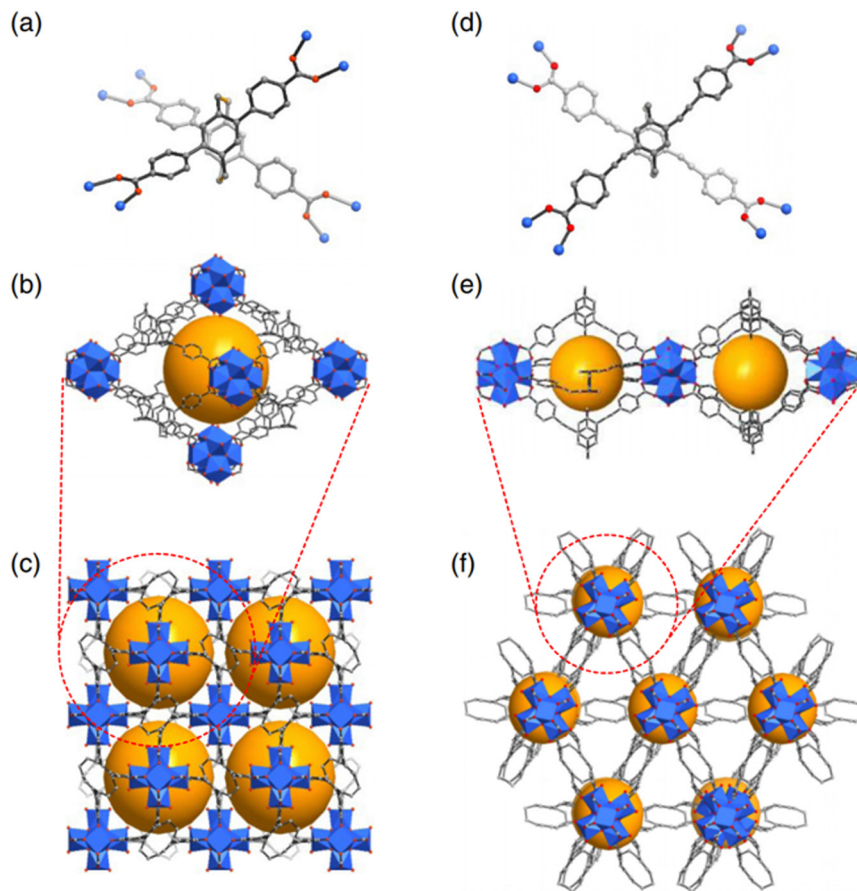


Fig. 5 Structures of  $L^1$  (a) and  $L^2$  (d) in pCp-1 and pCp-2; cages in pCp-1 (b) and pCp-2 (e); 3D porous structures of pCp-1 (c) and pCp-2 (f) viewed along the  $c$ -axis. The cavities are highlighted by yellow spheres.  $Zr_6$  cluster, blue polyhedron; C, grey; O, red. H was omitted for clarity.<sup>80</sup> Reproduced with permission from ref. 80. Copyright 2023 Chinese Chemical Society.

hierarchical regulation of the chirality communication characteristic facilitated the design of stimuli-responsive chiral sensors. Metal-mediated cages containing multiple cavities were prepared from  $Pd^{II}$  cations and tris- or tetrakis-monodentate bridging ligands.<sup>99</sup> A polycatenane was able to be formed by the overlap of neighboring cages (Fig. 6(B)). The peanut-shaped  $[Pd_3L_4^1]$  cage was quantitatively converted into its interpenetrated  $[5Cl@Pd_6L_8^1]$  catenated dimer. A basket-shaped triscationic cage was prepared by taking advantage of multivalence to avoid the labile property of imine.<sup>100</sup> This strategy facilitated the construction of more complicated catenanes and polycatenane structures.  $Mn(II)$  coordination polymers were synthesized depending on distinct polynuclear and polymeric chain units.<sup>101</sup> Two identical 3D networks were mutually interpenetrated with each other. Due to the existence of cages, a 3D 6-connected polycatenane framework was formed by utilizing interlinked dimeric  $[Mn_2O_2]$  units. The entangled coordination framework  $[Mn_4(sdba)_4(bim)(H_2O)_4] \cdot 2H_2O$  presented a parallel interpenetrating array with coexistence of polyrotaxane and polycatenane.<sup>102</sup> A chiral [2]catenane was synthesized based on the interlocking of trigonal bipyramidal cages containing three windows.<sup>103</sup> All six tris-chelated  $Zn(II)$  centers within [2]catenane possessed the same handedness, leading to the chirality of [2]catenane.

The cage-to-framework strategy has been proved to be efficient for enhancing the function-added values of cages and engineering their features and functions. The application of cages as nano-sized synthons provided new materials with unusual structural properties, chemical stability, and functions, such as selectivity, sensing capability, and catalytic efficiency. Novel cage-based framework designs have been mainly focused on improving chiral architecture separation, sensing, and catalysis performance. Self-sorting of POCs presents tremendous benefits in the fabrication of enantiorecognition materials. The cage-to-framework approach facilitates the formation of various chiral structures such as MOFs, HOFs, polymers, and polycatenanes. Furthermore, this cage-to-framework strategy enables the communication, transmission and amplification of chirality. Innovative cage-based frameworks for chiral applications are summarized in Table 1.

### 3. Design of chiral fractal nanomaterials

A fractal refers to a mathematical set that presents a self-similar pattern with a fractal dimension.<sup>104–109</sup> This fascinating shape can be fabricated based on simple mathematical rules that

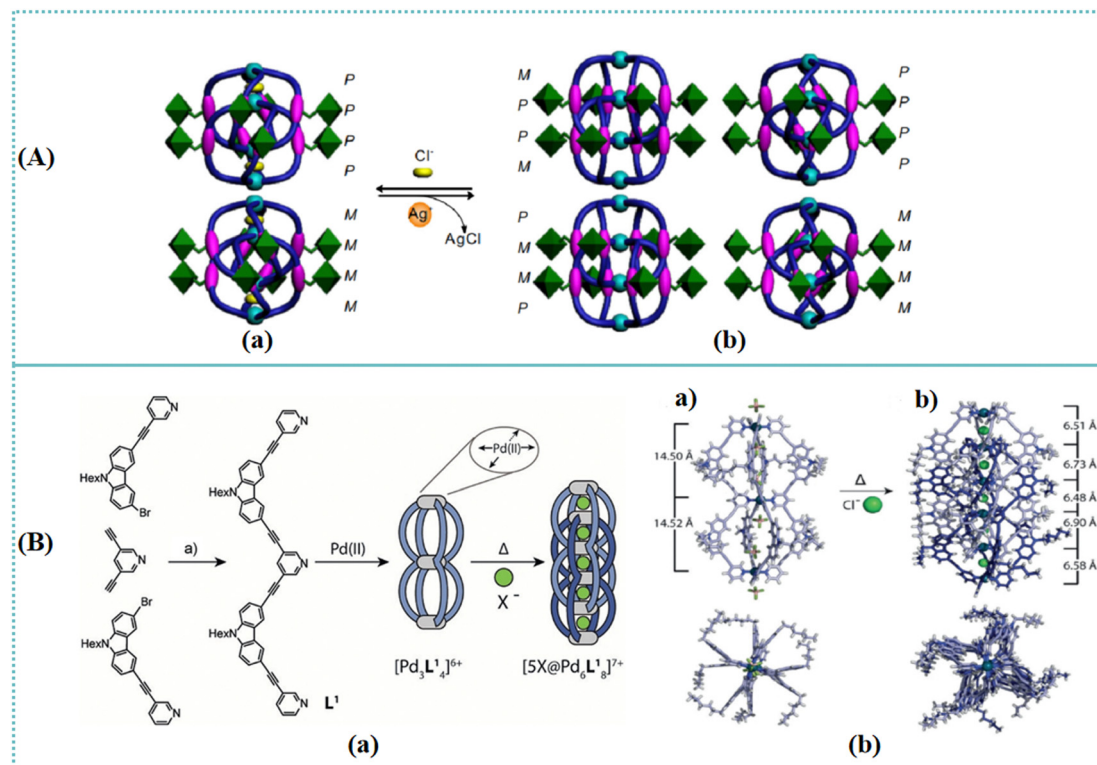


**Fig. 6** (A) Schematic representation of the chirality dynamics and hierarchical communication of the helicites. (a) Two conformations (PPPP and MMMM) of the dimeric helicites complexed with two  $\text{Cl}^-$  anions. (b) Four isomers (PPPP, MMMM, PMMP, and MPPM) of the dimeric helicites exist due to the communication between the ligands.<sup>98</sup> Reproduced with permission from ref. 98. Copyright 2021 Springer Nature. (B) (a) Synthesis of ligand  $\text{L}^1$ , assembly of the monomeric peanut cage  $[\text{Pd}_3\text{L}^1_4]^{6+}$  and halide-templated interpenetration to a double cage  $[\text{5X@Pd}_6\text{L}^1_8]$  ( $\text{X} = \text{Cl}^-$ ,  $\text{Br}^-$ ); (a)  $\text{CuI}$ ,  $\text{Pd}(\text{PPh}_3)_2\text{Cl}_2$ ,  $\text{NEt}_3$ ,  $90^\circ\text{C}$ . (b) Side view and top view of the single-crystal X-ray structures of (a) the monomeric peanut cage  $[\text{Pd}_3\text{L}^1_4]$  (counter anions =  $\text{BF}_4^-$ ) and (b) interpenetrated double cage  $[\text{5Cl@Pd}_6\text{L}^1_8]$  (counter anions outside the cage structure were omitted for clarity). Pd–Pd interatomic distances are shown. C light/dark violet; N blue; O red; Cl green; F light green; B pink; Pd green.<sup>99</sup> Reproduced with permission from ref. 99. Copyright 2018 John Wiley and Sons.

contribute to structures with distinguished complexity and beauty.<sup>110</sup> Fractals commonly exist in nature. For instance, Sendker *et al.* discovered a natural metabolic enzyme, citrate synthase from the cyanobacterium *Synechococcus elongatus*, which self-assembles into Sierpiński triangles (STs). Fractal nanomaterials have been considered a favourable alternative for chirality transmission due to the self-similar feature of a fractal. Tree-shaped fractal materials facilitate the hierarchical

chirality transference at multiple levels. Fractal chirality of bone minerals, *Escherichia coli* bacteria aggregation, and organic molecular cages are described as well. Based on the prominent advantages of nanomaterials, different types of fractal nanomaterials can be utilized for asymmetric catalysis. Various nanomaterials including single-walled carbon nanotubes (SWCNTs), gold nanomaterials, and silica nanoparticles are favourable choices for developing chiral fractal structures.

**Table 1** Advantages of using chiral cage-based frameworks

Types of cages	Types of frameworks	Advantages	Applications	Ref.
Porous organic cages	Self-sorting of cages, catenanes	Structural reversible transformation	Enantio-recognition of enantiomers	42, 56 and 57
Porous coordination cages	Cage-in-cage frameworks, hierarchically porous assembly	Multichiral microenvironment	Chiral separation of drug intermediates	75 and 76
Porous coordination cages	Microporous frameworks	Chiral transference and amplification	Enantio-recognition and separation of enantiomers	77–79
Metal organic cages	Metal–organic frameworks	Improved efficiency, chiral transference	Chiroptical materials	80–84
Metal organic cages	Hydrogen-bonded organic frameworks	Improved structural stability	Chiral catalysis	85 and 86
Porous coordination cages	Coordination polymers	Improved cages internal cavity accessibility	Enantio-recognition	87 and 88
Metal organic cages	Interpenetrated helicate structures, polycatenanes	Chirality communication	Chiral sensing and recognition	98–103

Moreover, biomolecules such as cellulose, chitosan, and protein provide an efficient alternative for the construction of fractal nanomaterials.

Among a variety of prototypical fractals, the ST was usually used as a decorative pattern in tiling mosaic floors in a medieval Rome mathematical set. A series of planar molecular STs was prepared based on self-assembly at the Ag(111) surface by choosing two aromatic bromo compounds (4,4''-dibromo-1,1':3',1''-terphenyl (B3PB) and 4,4'''-dibromo-1,1':3',1''-4'',1'''-quaterphenyl (B4PB)) as building blocks.<sup>111</sup> Different from the symmetric STs, the resulting molecular STs possessed clockwise (CW) or counterclockwise (CCW) chirality (Fig. 7(A)). This ST orientation relative to the Ag(111) substrate lattice played an important role in generating chirality. Chirality was able to be transferred from one cyclic halogen bonding node to all the nodes in the whole molecular fractal due to the specific self-similar property of a fractal. This study provided an efficient

strategy for preparing plentiful planar molecular fractals at surfaces. Zhang *et al.* prepared tree-shaped fractal patterns by self-assembly of the *N*-[(9*H*-fluoren-9-ylmethoxy) carbonyl] protected glutamic acid (Fmoc-Glu) and zinc-porphyrin (ZnTPyP).<sup>112</sup> Depending on the synergistic interaction of  $\pi$ - $\pi$  stacking, hydrogen-bonding, and coordination between zinc ion with a pyridyl moiety, the nanorod structures were obtained for the co-assemblies. Left- and right-handed arrangement of nanorods and fractal patterns were formed based on *L*-Fmoc-Glu and *D*-Fmoc-Glu, respectively (Fig. 7(B)). As an important unit of the fractal patterns, the nanorods were aggregated one-by-one in a single direction. The hierarchical chirality transference was realized at multiple levels. First, the molecular chirality was transferred from glutamic acid to porphyrin chromophores. Furthermore, the spiral-stacked nanorod structures constructed chiral architectures. These structural features of the spiral fractal patterns offered innovative insight into the design of

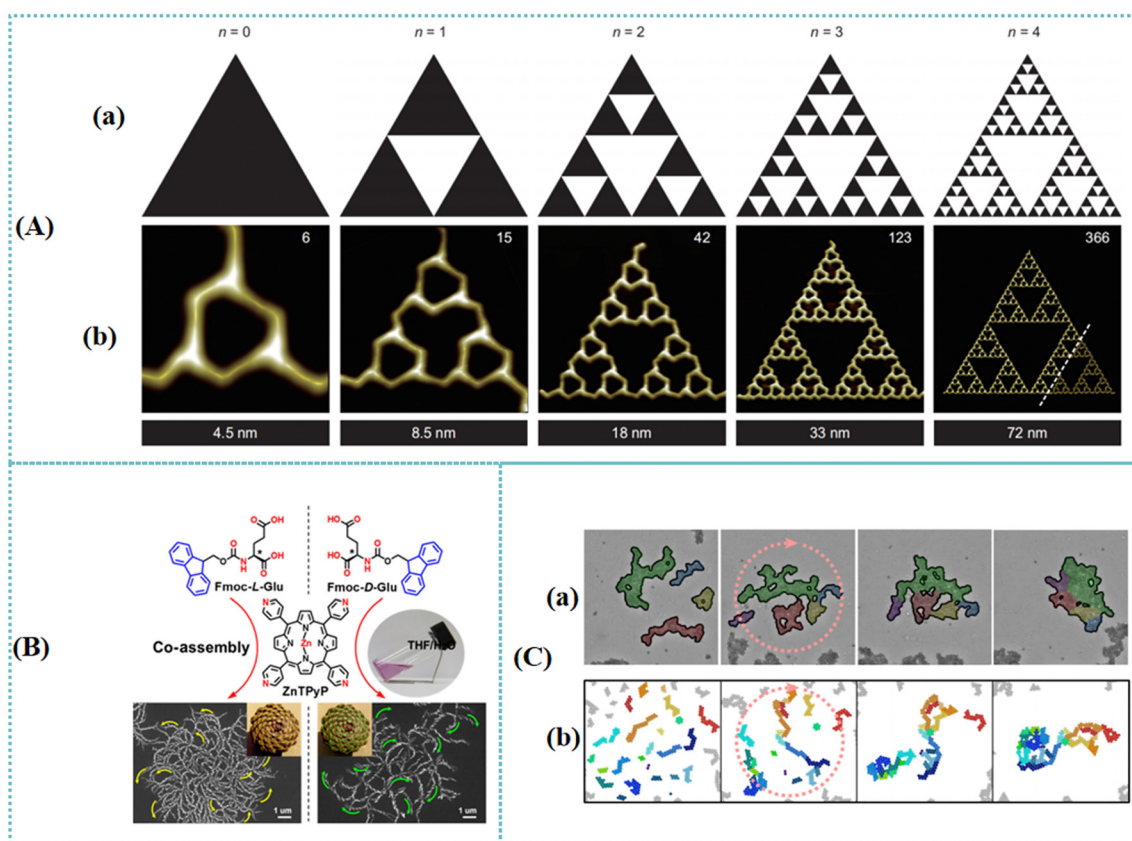


Fig. 7 (A) The whole family of the observed B4PB molecular STs. Models of the STs (a) and the corresponding STM images of B4PB-ST- $n$  ( $n = 0, 1, 2, 3$  or 4) (b). The number in each image in (b) indicates the number ( $T_n$ ) of the B4PB molecules that participate in the corresponding molecular ST. The STM image for  $n = 4$  (b) is a cropped section of an imperfect B4PB-ST-4 structure (the largest one achieved in experiments to date). To illustrate the ST-4 structure clearly, the missing bottom-right corner, separated by the dashed line, was artificially added to the structure and is composed of modelled molecules. The length given below each STM image in (b) indicates the horizontal size of the corresponding STM image.<sup>111</sup> Reproduced with permission from ref. 111. Copyright 2015 Springer Nature. (B) A route for the preparation of chiral fractal patterns. Top: Molecular structures of the *L/D*-Fmoc-Glu and ZnTPyP. Bottom: After assembling Fmoc-Glu with ZnTPyP in mixed solvent of THF/ $H_2O$ , chiral fractal patterns composed of nanorod structures were obtained and those nanorods arranged in a spiral sense, which were controlled by the absolute configuration of Fmoc-Glu. *L*-Fmoc-Glu caused the anticlockwise arrangement of nanorods, as marked by a yellow arrow, while clockwise arrangement of nanorods was obtained in the case of *D*-Fmoc-Glu.<sup>112</sup> Reproduced with permission from ref. 112. Copyright 2022 Springer Nature. (C) Rotation and folding of aggregates. Rotation and folding of aggregates in experiments (a) and simulations (b) leading to compaction of the aggregates in an active bath.<sup>114</sup> Reproduced with permission from ref. 114. Copyright 2023 Springer Nature.

hierarchical chiral materials. Chirality is an important attribute of organisms. As a vital part of organisms, bone composing apatite and collagen fibrils possessed chirality. Nine levels of fractal-like chirality of bone minerals from the atomic to macroscopic scales were investigated by employing electron microscopic and spectrometric characterizations.<sup>113</sup> Secondary helical subplatelets were formed based on the lateral merging of the primary helically twisted acicular apatite crystals inside collagen fibrils and between fibrils. Furthermore, chiral arrangement of subplatelets led to tertiary spiral mineral platelets. Quaternary to ninth levels were obtained depending on the coherent stepwise stacking of mineral platelets with collagen fibrils. The hierarchical chirality structure presented desirable optical activities with a wide-band electromagnetic wave response. The exploration of this chiral structure offered novel insight into developing artificial chiral inorganic materials. Unconventional colloidal aggregation in chiral *Escherichia coli* bacteria was investigated by Palacci *et al.*<sup>114</sup> A persistent rotation of the aggregates was caused by the chirality of the *Escherichia coli* flagella. The morphology and statistical properties of the aggregates formed in the baths were investigated. Depending on the fraction of colloids at the perimeter, aggregates that formed in the thermal and active baths were classified into different groups. Due to the observed rotation, the non-equilibrium properties were obtained based on the compaction and folding of the aggregates (Fig. 7(C)). The fractal dimensions of an ensemble of aggregates were calculated for quantifying the morphological changes. A physical model was developed to explore the chirality of the bacterial bath. The results suggested that the clockwise rotation of the beads was achieved *via* an internal driving torque. The difference between aggregation in the active and thermal baths was explored by using the numerical simulations. This work highlighted the essential role of active baths in constructing the structural and mechanical characteristics of materials with unconventional phases. In addition to biological macromolecules, high-level chiral organic molecular cages with fractal superstructures were also developed. A racemic 3D tri-bladed propeller shaped helical molecular cage was synthesized by utilizing 2D tri-bladed propeller shaped triphenylbenzene as building blocks.<sup>115</sup> Higher-level 3D tri-bladed chiral helical molecular cages with multilayer sandwich structures were further prepared by choosing 3D molecular cages as building blocks. The resulting molecular cage enabled the formation of L/D-helical nanofiber supermolecule architectures. The scale transformation of chirality from atoms to trihelical cages and then to spiral nanofibers was realized.

Hierarchically organized chiral particles were prepared depending on polydisperse gold thiolate nanoplatelets with cysteine as the surface ligands.<sup>116</sup> The topological elements of these particle's geometry were able to be replicated with distinct degrees of similarity. The complicated organization was derived from competing chirality-based assembly restrictions that render assembly approaches primarily dependent on nanoparticle symmetry. The resulting particles with specific optical, chemical, and colloidal characteristics presented promising potential in optoelectronics and asymmetric catalysis. Peptide-based functional nanomaterials have attracted increasing attention in the biomedicine field.<sup>117</sup>

Various approaches have been applied for directing the self-assembly of peptide building blocks. The self-assembly peptide amyloid-like structure was developed to investigate the effect of nanostructure morphologies on stereoselective aldol reactions. The resulting compounds that compose the fractal aggregates possessed larger size. The chiral assemblies' folding arrangement in the polypeptide chains played an important role in the catalysis process. Fractal-like aggregates were able to be formed by self-assembly of short peptides.<sup>118</sup> The influence of catalytic action and specific ion effect on hydrogelator formation was explored. Results suggested that the kosmotropic ions facilitated the open and dynamic fractal networks, whereas the chaotropic ion induced a dense mass fractal structure.<sup>119</sup> The chirality and mechanical characteristics of the proposed gel-phase materials were affected by the differential hydrophobic interactions. Bigall *et al.* synthesized the porous and lightweight aerogels of shape-controlled Pt nanomaterials including nanospheres and nanocubes.<sup>120</sup> The random coalescence of the individual nanocrystals induced porous fractal type networks of the aerogels. For instance, the Pt nanocubes were interconnected by sharing their lattice points, inducing the formation of a Pt-Pt metal bond between two nanocrystals. Asymmetric hydrogenation of keto-pantolactone was realized by using the gels as catalysts. The nonsurface modified SWCNTs referred to carbon allotropes defined by the chiral angle and length of the tube roll-up vector.<sup>121</sup> The influence of SWCNT's electronic structure (features of chiral wrapping angles and diameter) on lung epithelial cells infectivity by pandemic influenza A H1N1 virus was explored. The aggregate structure was evaluated by determining fractal dimension. The results suggested that chirality was able to affect both fractal structure and aggregation of SWCNTs. Fractal dimension was considered an important factor for influencing biological interaction of SWCNTs.<sup>122</sup> The distinct surface energies of SWCNTs impacted the binding of these nanoparticles to biomolecules, further influencing viral infectivity. In addition, fractal dimension measurement enabled the evaluation of SWCNT aggregates' stability in gum arabic.<sup>123</sup> The extending branches on the gold seeds facilitated the formation of fractal nanostructures.<sup>124</sup> Silica nanoparticles were also able to form a fractal network *via* the gelatin conformational transition.<sup>125</sup> Among various biological nanomaterials, nanocellulose attracted tremendous interest in the material science field. Cellulose nanocrystals were considered a desirable chiral building block material. Nyström *et al.* utilized the aggregated carboxymethylated cellulose nanocrystals to construct larger chiral fractal structures.<sup>126</sup> Amphiphilic carboxymethyl-hexonoyl chitosan nanoparticles were also developed.<sup>127</sup> A fractal transition between nanoparticulate and short fiber-like network evolution of carboxymethyl-hexonoyl chitosan was observed as time elapsed. A fractal aggregate was prepared by choosing protein cage nanoparticles as building units.<sup>128</sup>

A variety of fractal nanomaterials can be applied for chirality transference. Tree-shaped fractal patterns utilized for the hierarchical chirality transference are highlighted. Increasing attention has been paid to the multiple levels of bone mineral fractal chirality and fractal dimensions of chiral *Escherichia coli* bacteria aggregation. Fractal-like nanomaterials present specific advantages in constructing biocatalysts. Noteworthy efforts

Table 2 Advantages of using chiral fractal nanomaterials

Types of fractal nanomaterials	Advantages	Applications	Ref.
Sierpiński triangle	Chiral transference	Chiral recognition	111
Tree-shaped fractal patterns	Hierarchical chirality transference	Chiral recognition	112
Polydisperse gold thiolate nanoplatelets	Chiral transference	Optoelectronics and asymmetric catalysis	116
Peptide-based functional nanomaterials	Chiral transference	Chiral catalysis	117 and 118
Platinum nanocubes	Chiral transference	Chiral catalysis	120
Cellulose nanocrystals	Chiral transference	Chiral recognition	126
Full color circularly polarized luminescence nanoflowers	Chiral transmission	Circularly polarized luminescence materials	141
CuO nanoflowers	Signal amplification	Chiroptical applications, electrochemical sensing	143 and 169
CdSe/CdS core-shell nanoflowers	Chiral transference	Circularly polarized luminescence materials	144
Nanoflowers containing films	Chiral amplification	Chiroptical applications, chiral recognition	147, 149, 150 and 177
Gold nanoflowers	Chiral transmission	Chiral plasmonic nanomaterials, surface-enhanced Raman scattering, electrochemical sensing	160, 161 and 170
Silver nanoflowers	Signal amplification	Surface-enhanced Raman scattering	165 and 166
Enzyme-immobilized nanoflowers	Enhanced catalytic activity and stability	Chiral catalysis	171–176

have been made to develop different types of chiral fractal nanomaterials. Novel fractal nanomaterials employed for chiral applications are summarized in Table 2.

## 4. Design of chiral nanoflowers

When applied to flowers, fractals can capture the arrangement of petals. Flower-like patterns that exhibit self-similarity are able to be created by using mathematical algorithms inspired by fractals.<sup>129–133</sup> The design of chiral nanoflowers has received considerable interest due to their potential application in various domains such as material science, biosensing, biocatalysis, and enantioselective recognition at the cellular level. Chiral nanoflowers provide desirable alternatives for developing chiroptical materials. Many efforts have been focused on investigating chirality transference and amplification based on nanoflowers. To construct satisfactory biosensors, nanoflowers have been efficiently applied in electrochemical sensing. The flower-shaped morphology of nanoflowers provide them with a large surface-to-volume ratio and enhanced catalytic activity. Enzyme-based nanoflowers facilitate the immobilization of enzymes without harsh conditions and the improvement of enzymes performance. The high surface area and stability of nanoflowers enable improved optical response, enzymatic activity, and further potential applications in optoelectronics, sensors, bioelectronics, catalysis, and drug delivery.

### 4.1 Designing chiral nanoflowers for chiroptical application

Chiral nanoflowers can provide a desirable platform for chiroptical application. Novel fabrication strategies have been mainly focusing on achieving chiral transfer, sensitivity enhancement, and signal amplification. Various types of chiral nanoflowers have attracted much attention for use in developing CPL materials. In addition, the optical activity of chiral nanoflower-based films is described in this section. Gold nanoflowers are satisfactory choices for developing chiral plasmonic nanomaterials. Moreover, state-of-the-art chiral nanoflowers applied for Raman improvement are reviewed.

CPL materials have attracted tremendous attention in materials science and chirality-related applications.<sup>134–140</sup> Due to their multi-color CPL emissions, full-color CPL-active materials present specific advantages in practical applications. Compared with traditional tedious preparation strategies, Deng *et al.* exploited a simple and universal CPL materials preparation method.<sup>141</sup> Nanoarchitectures including chiral inorganic nanoflowers, organic–inorganic hybrid nanoflowers, and organic polymer nanofibers were combined with achiral fluorescence dyes for developing full-color CPL materials (Fig. 8(a)). The unpolarized fluorescent light was able to be transformed into CPL by utilizing these nanoarchitectures as handed-selective fluorescence filters. Organic–inorganic chiroptical materials possessed specific merits in chiral applications.<sup>142,143</sup> Cellulose nanocrystal (CNC) was applied as a chiral template for developing chiral CuO@CNC nanoflowers. The resulting CuO@CNC nanoflowers were further combined with the achiral fluorescent dyes for the CPL test, and intense CPL signals were observed. Moreover, chiral CuO nanoflowers were synthesized by calcination of CuO@CNC nanoflowers. The results indicated that the direction of CPL signals in CuO nanoflowers was obviously different.

To confirm the significance of chiral elements in constructing CPL materials, the achiral CuO nanoparticles were used for the CPL test, and the CPL signal disappeared. This work provided an efficient approach for developing various chiroptical functional materials.

Attributing to their tunable quantum confinement function, ligand-induced chirality in CdSe/CdS core-shell nanocrystals (NCs) has been widely utilized in chiral biosensing, CPL, and chiroptic-based devices. He *et al.* synthesized a series of CdSe/CdS core-shell NCs with various anisotropic shapes such as nanoflowers, tadpoles, and dot/rods (Fig. 8(b)).<sup>144</sup> To explore the relationship between nanomaterial geometries and NC chirality, circular dichroism (CD) and CPL spectrometers were applied for evaluating the induced chiroptical characteristics of the nanostructures. It was found that the chiral ligand–photoluminescent core interactions played an essential role in indicating CPL performance. Depending on this study, a facial method was developed for synthesizing different types of CdSe/

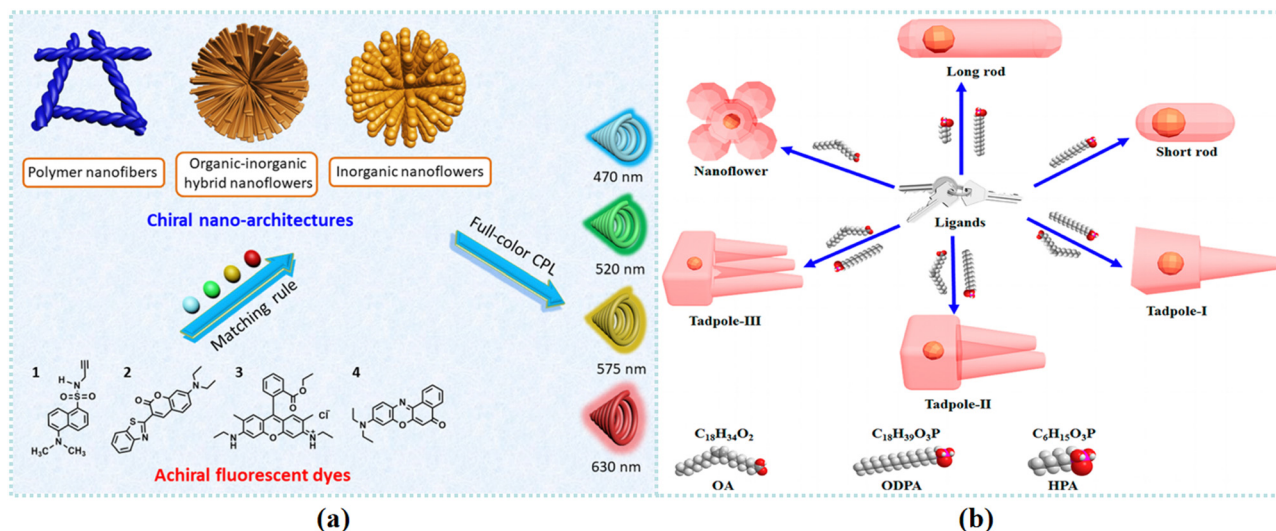


**Fig. 8** (a) Schematic illustration for preparing full-color CPL materials by taking chiral nanoarchitectures as handed selective fluorescence filters.<sup>141</sup> Reproduced with permission from ref. 141. Copyright 2020 American Chemical Society. (b) Mechanism of ligand-induced shape variations. By changing the composition of the ligands, various anisotropic shapes such as nanoflowers, tadpoles with one to three tails, and dot/rods can be obtained.<sup>144</sup> Reproduced with permission from ref. 144. Copyright 2020 American Chemical Society.

Cds nanostructures with tunable CD and CPL activities. To investigate the interaction between dimensional morphology transition and signal transfer functions, multidimensional nanostructures with optimizable CPL were also prepared by using the self-assembling positively charged chiral  $\pi$ -building block.<sup>145</sup> This research offered an efficient method for understanding signal communication and transportation in natural systems. The photocontrolled conversion of morphology and transferred chirality were also investigated depending on snowflake-like supramolecular clockwise-helical assembly.<sup>146</sup>

Mesostructured  $\text{NiFe}_2\text{O}_4$  films with numerous nanoflowers were prepared to investigate their chirality induced spin selectivity. In these ferrimagnetic materials, each nanoflower was assembled from nanoplates (Fig. 9(A)).<sup>147</sup> When choosing *L*-tyrosine as the symmetry-breaking agent, the nanoplate's arrangement induced the formation of a counter-clockwise circinate morphology. Nevertheless, the *D*-films displayed the opposite direction. A variety of chiral nanomaterials including carbon nanotubes, MOFs, and ligand-capped CdSe quantum dots were utilized in spin devices to realize the chiral-induced spin selectivity.<sup>148</sup> We foresee a growing interest to chiral nanoflowers in spins electronics. Moreover, different nanoflower-based films were designed for chiroptical applications. Duan *et al.* synthesized chiral mesostructured  $\text{TiO}_2$  films by utilizing *L*/*D*-mannitol as the symmetry-breaking agent.<sup>149</sup> The resulting  $\text{TiO}_2$  films possessed a hierarchical chiral structure (Fig. 9(B)). First, nanoparticles were formed based on primary distorted crystal lattices. Chiral stacks of nanoparticles further constructed bamboo-like nanorods. Subnanoplates composed of tertiary nanorods were able to fabricate quaternary chiral nanoplates. Finally, quinary nanoflowers were obtained depending on helically arranged nanoplates. According to the signals of optical activity, these films developed with *D*- and *L*-mannitol were demonstrated to be left-handed and right-handed materials,

respectively. The optical properties of silver chiral nanoflower sculptured thin films were also investigated.<sup>150</sup>

Chiral plasmonic nanomaterials have attracted increasing attention due to their improved optical chirality in the visible and near-infrared region.<sup>151</sup> By investigating their localized surface plasmon resonances, chiral plasmonic nanomaterials such as gold, silver, magnesium and alloyed materials can be employed for chemical sensing.<sup>152</sup> Biomolecule-mediated chiral nanomaterials are widely utilized in enantioseparation and chiral biosensing due to their advantageous biological and optical characteristics.<sup>153</sup> Inorganic nanoparticles can be coated with DNA to construct chiroplasmonic assemblies without an aggregation tendency.<sup>154</sup> A variety of chiral-shaped gold nanoparticles were prepared *via* chiral molecule-mediated strategies.<sup>155–157</sup> For instance, Zheng *et al.* prepared chiral  $\text{Au}_{20}$  nanoclusters by using a surface/interface solidification strategy.<sup>158</sup> The obtained nanoclusters presented an almost 40-fold improvement of chiroptical activity when compared with  $\text{Au}_{19}$ . Additionally, gold deposition on gold seeds was able to construct chiral nanostructures under the control of chiral glutathione and in the presence of hexadecyltrimethylammonium bromide.<sup>159</sup> Among distinct plasmonic gold nanoparticles, branched gold nanoparticles possess tremendous potential based on their large surface-to-volume ratio and satisfactory surface plasmon resonance characteristics. Gold–glutathione complexes were synthesized by combining the glutathione oligomers with gold.<sup>160</sup> The chiral morphology of gold nanooctopods (NOPs) was adjusted by optimizing the amount of glutathione oligomers. The results indicated that a higher glutathione oligomerization degree facilitated the formation of flower-like chiral nanoparticles. These nanoflowers were able to be obtained after the regrowth of gold NOPs with the glutathione incubated for three days (Fig. 10). The morphology changes of F-NPs were consistent with their extinction and CD spectra, suggesting that the chirality was triggered by the

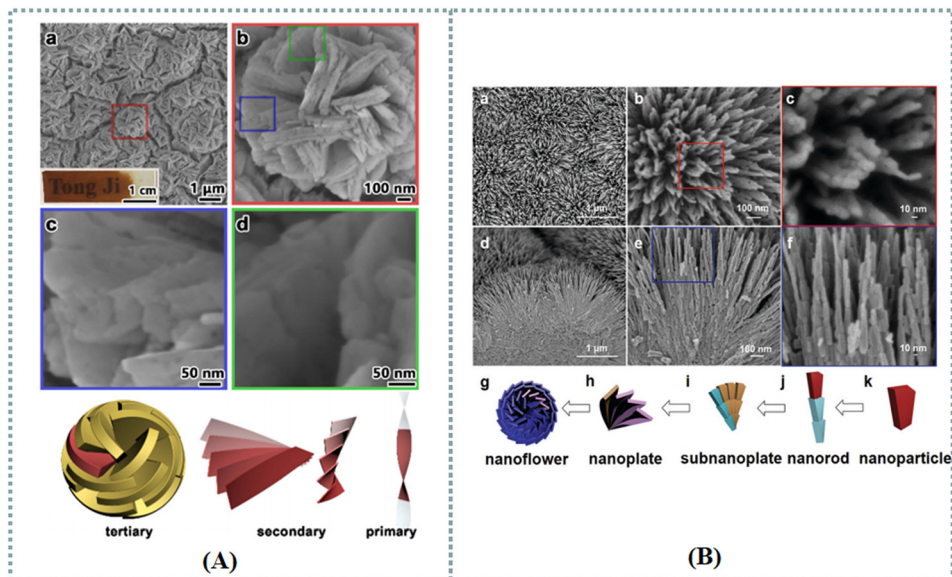


Fig. 9 (A) SEM images of an L-CMNFF with varying magnifications, and schematic drawings of the hierarchically chiral structures in L-CMNFFs.<sup>147</sup> Reproduced with permission from ref. 147. Copyright 2023 Royal Society of Chemistry. (B) Top-view (a)–(c) and side-view (d)–(f) SEM images of an L-CMTF with varying magnifications, a schematic drawing of the hierarchical chirality in L-CMTFs (g)–(k).<sup>149</sup> Reproduced with permission from ref. 149. Copyright 2020 Royal Society of Chemistry.

shape of nanoflower chiral structures. Depending on this work, chiral plasmonic nanomaterials with optimizable chiroptical properties presented specific advantages in the field of optical materials and chiral catalysis.

Chiral gold nanoflowers with petal-shaped tips were prepared by choosing L-ascorbic acid as a chiral reducing agent in the presence of chiral guanosine 5'-monophosphate.<sup>161</sup> These nanoflowers displayed suitable biocompatibility for cellular dark-field imaging and photothermal therapy. Due to the abundant 'hot spots' produced by their special surface geometry, the proposed nanoflowers were also considered ideal surface-enhanced Raman scattering (SERS) substrates. Though Raman spectroscopy can deliver molecular structure information, Raman signals usually present weak intensities and low sensitivities. Therefore, a SERS technique has been applied in analytical chemistry to enhance Raman signals.<sup>162–164</sup> The metal-based nanomaterials are favorable SERS platforms with satisfactory signal enhancement performance. Silver nanoflower thin films with distinct symmetries were developed on copper substrates.<sup>165,166</sup> A high degree of Raman spectroscopy signal enhancement was observed when using the prepared materials for 4,4'-bipyridine detection. It was supposed that nanoflowers with longer and narrower petals facilitated signal enhancement. In addition to metal-involved materials, metal-free nanomaterials possessed specific advantages for Raman enhancement. Polyaniline (PANI)-based rose-like chiral nanostructures were developed based on the oxidation polymerization of aniline occurring in a reaction droplet.<sup>167</sup> Due to cavity-shaped and chiral structured properties of rose-like nanostructures, the resulting metal-free materials presented a desirable Raman enhancement performance.

#### 4.2 Designing chiral nanoflowers for electrochemical sensing

The broad application of nanoflowers promotes interest in electrochemical sensing. New chiral nanoflowers for fabricating

electrochemical sensors are reviewed. Noteworthy efforts have been made to improve the recognition efficiency, specificity, and stability of nanoflower-based chiral sensors. The merits of applying chiral nanoflowers for electrochemical sensing are highlighted in this article.

To realize the chiral recognition of tryptophan with achiral glycine, L-CuO was applied for decorating glycine (Gly) *via* the formation of a Cu(Gly)<sub>2</sub> complex.<sup>168</sup> First, L-CuO was developed

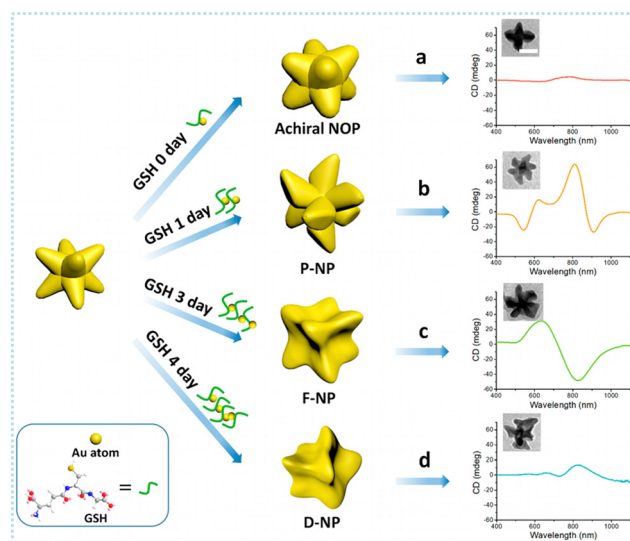


Fig. 10 Schematic of the synthesis of different-morphology Au NPs. (Right) CD spectra of Au NPs prepared with L-GSH with different incubation times: (a) 0 days, (b) 1 day, (c) 3 days, and (d) 4 days. (insets) Representative transmission electron microscopy (TEM) images of AuNPs. Scale bar: 50 nm.<sup>160</sup> Reproduced with permission from ref. 160. Copyright 2021 American Chemical Society.

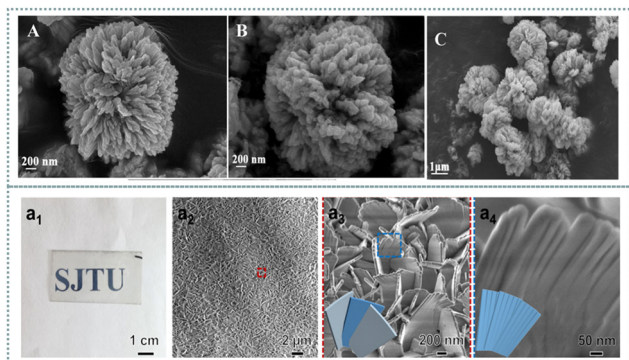


Fig. 11 FESEM images of L-CuO (A) and L-CuO-Gly (B) and (C).<sup>168</sup> Reproduced with permission from ref. 168. Copyright 2020 American Chemical Society. Morphology and chiral structure of L-CMHAPFs. (a<sub>1</sub>)–(a<sub>4</sub>), Photographs and SEM images of L-CMHAPFs at varying magnifications.<sup>177</sup> Reproduced with permission from ref. 177. Copyright 2022 American Chemical Society.

by choosing *S*-2-amino-3-phenyl-1-propanol as the symmetry-breaking agent. The resulting L-CuO possessing a peony-like morphology was assembled with densely arranged nanopetals grown from the center of the flower (Fig. 11). A rotation of contort petal aestivation provided the L-CuO nanoflower with chirality. The chirality transfer method was employed for providing Gly with chirality. After incorporating L-CuO with achiral Gly, the nanopetals were still stacked in a single direction, indicating the intrinsic chirality of L-CuO-Gly. The obtained L-CuO-Gly-modified glassy carbon electrode was used for recognizing tryptophan isomers depending on the chirality and specific steric configuration of L-CuO. The enhanced recognition efficiency of this sensor was observed due to the hydrogen bonds between tryptophan and Gly. The quantitative assay of tryptophan isomers was also able to be achieved by using this sensing platform. Nanoflower-based materials presented specific merits in electrochemical sensing.<sup>169</sup>

Multi-enzyme-labeled gold nanoflowers were selected as signal enhancers in the fabrication of a multi-walled carbon nanotube-poly(L-lysine) modified electrochemical immunosensor for ofloxacin.<sup>170</sup> Compared with spherical gold nanoparticles, the gold nanoflowers with branches were much more useful for preparing a multi-enzyme label. This sensor displayed desirable specificity, stability and reproducibility.

### 4.3 Designing chiral nanoflowers for biocatalysis

In addition to being used as biosensors, enzyme-immobilized nanoflowers were considered satisfactory biocatalysts for producing biochemicals.<sup>171</sup> In contrast to other enzyme-immobilized catalysts, the nanoflower-based reactor displayed enhanced catalytic activity and stability. The coenzyme NADP<sup>+</sup> and enzymes including conjugated polyketone reductase and glucose dehydrogenase were encapsulated in organic-inorganic hybrid nanoflowers for asymmetrically reducing ketopantolactone to produce *R*-(-)-pantolactone. This reactor presented desirable stereoselectivity, thermostability, and reusability.<sup>172</sup> As a type of cofactor-dependent enzyme,  $\omega$ -transaminase

possessed favourable catalytic activity for producing chiral amines. To increase enzyme stability, a self-sufficient biocatalyst was developed by coimmobilizing  $\omega$ -transaminase and cofactors into nanoflowers.<sup>173</sup> *Brevibacterium* cholesterol oxidase-copper hybrid nanoflowers with an improved conversion ratio exhibited promising potential in steroid derivative bioconversion in the pharmaceutical industry.<sup>174</sup> Carbon nanotube-lipase hybrid nanoflowers possessed enhanced enzyme activity and enantioselectivity.<sup>175</sup> Moreover, chiral gold nanoflowers without enzymes were also able to be used as catalysts.<sup>176</sup>

Various chiral nanoflowers can be applied for developing new biocatalysts. Enzyme-based nanoflowers exhibit substantial advantages in asymmetric catalysis. These hybrid nanoflowers facilitate the improvement of enantioselectivity and stability. Additionally, nanoflowers without enzymes used for catalysis are described as well.

### 4.4 Designing chiral nanoflowers for cell related applications

Chiral nanoflowers provide a promising alternative for cell related applications. The advantages of utilizing nanoflowers for exploring the recognition interaction between cells and chiral materials have been described in this section. Distinct nanoflowers are considered efficient cell markers and drug delivery reagents. Moreover, DNA nanoflowers used for drug delivery are highlighted.

Since cells with a chiral hierarchical organization prompted the homochirality of organisms, it is essential to exploit the recognition between cells and chiral materials. Tartaric acid was utilized as a symmetry-breaking agent for fabricating inorganic chiral mesostructured hydroxyapatite films (CMHAPFs).<sup>177</sup> The film containing dense nanoflower arrays presented five levels of fractal-like chirality (Fig. 11). Flowers consisting of helically stacked nanopetals formed the quinary-level chirality. The quaternary-level chirality was attributed to the helical arrangement of nanoplates in the nanopetals. Furthermore, tertiary nanoplates were composed of helically arranged nanoflakes, and secondary nanoflakes were formed based on nanoneedles. The primary chirality was obtained due to the twisted crystal lattice in the nanoneedles. This inorganic film was applied for exploring the enantioselective interactions between cells and chiral materials. CMHAPFs prepared with *L*-tartaric acid exhibited desirable performance in cell adhesion, cell proliferation, and osteogenic differentiation of primary mesenchymal stem cells, whereas CMHAPFs synthesized with *D*-tartaric acid displayed the opposite effect. This phenomenon was due to the stereo matching between multilevel chiral CMHAPFs mesostructures and hierarchical chiral cell surfaces.

In addition to investigating the interaction between chiral materials and cells, flower-like structures were used as a cell marker and drug delivery agent. The naphthalene diimide-lithocholic acid derivative self-assembled into a chiral flower-like morphology.<sup>178</sup> These structures possessed satisfactory biocompatibility and cellular uptake in cancerous cells. The self-assembly of chiral synthons was triggered by non-covalent interactions, and these interactions regulated the supramolecular chirality in self-assembled architectures. Chiral assemblies presented specific advantages in chiral separation, asymmetric

catalysis, and chiroptical materials. To develop controllable chiral nanoflowers has gained tremendous interest. Biomolecules such as DNA and monosaccharides were able to be used for developing chiral flower-like structures.<sup>179</sup> Due to their high specific surface areas, these materials were applied in optical enantioseparation, chiral sensing and separation, catalysis, and drug delivery system. DNA nanostructures facilitated the exquisite control of components on the nanoscale due to oligonucleotides' high programmability and predictability. The DNA nanoflowers were self-assembled by the liquid crystallization of replicated DNA building blocks. This type of nanoflower presented promising potential in drug delivery.

Substantial advances have been made in designing novel chiral nanoflowers. A variety of chiral nanoflowers can be designed for developing chiroptical materials, electrochemical sensors, and biocatalysts. Nanoflowers based on CuO and CdSe/CdS present specific benefits in constructing CPL materials. The optical activity of different films containing numerous nanoflowers has been investigated. Gold nanoflowers are considered satisfactory chiral plasmonic nanomaterials with adjustable chiroptical features. The combination of chiral nanoflowers with a SERS technique facilitates the enhancement of Raman signals. Chiral nanoflowers can also improve electrochemical sensors' enantio-recognition efficiency. Biocatalysts based on hybrid nanoflowers exhibit improved asymmetric catalytic activity and stability. In addition to recognizing chiral molecules, the nanoflowers' enantio-recognition ability at the cellular level is also described. In the exploration of drug delivery systems, the use of DNA nanoflowers has attracted tremendous research interest. Novel nanoflowers applied for chiroptical application, electrochemical sensing, biocatalysis, and cell related applications are summarized in Table 2.

## 5. Conclusions

A variety of self-similar chiral nanomaterials developed using an individual-to-family approach can realize chiral communication, transmission, and amplification. We reviewed the design and application of self-similar nanomaterials for chiral recognition, chiral catalysis and sensing, enantioseparation, and chiral optics (Fig. 12).

A remarkable effort has been devoted to designing cage-based extended frameworks. The marriage of cages provides new opportunities for developing self-similar chiral materials. Self-sorting of POCs presents substantial advantages in constructing favourable enantio-recognition materials. Moreover, MOCs are considered desirable building blocks to fabricate different types of chiral frameworks including MOFs, HOFs, polymers, and polycatenanes. We found that innovative 'cage-in-cage' frameworks based on MOCs can exhibit significant virtues for chiral separation. Moreover, polycatenanes utilized for chiral applications have been described in detail. Future research studies must explore cage-based interpenetrated architectures for chiral communication. Since extended frameworks display their superiority over individual cages, we foresee a growing interest to various cage-based extended frameworks in chiral transmission and amplification.

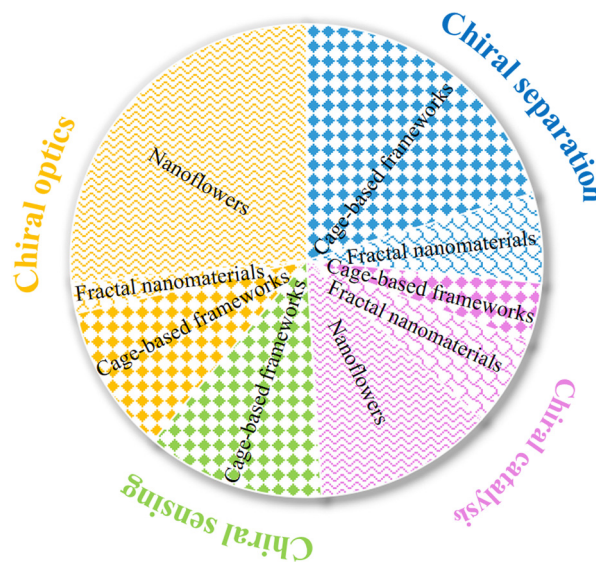


Fig. 12 Summary review of various self-similar nanomaterials applied for chiral catalysis and sensing, enantioseparation, and chiral optics.

The diversity of chiral fractal nanomaterials summarized in this review suggests that the self-similarity of a fractal facilitates the transmission and amplification of chirality. The fractal family tree possesses tremendous potential for realizing hierarchical chiral transmission at multiple levels. Fractal chirality of bone minerals and *Escherichia coli* bacteria aggregation has been described in detail. Studies indicate that chiral fractal nanomaterials are suitable for asymmetric catalysis. Considering the noteworthy merits of nano-biomaterials, we believe that much more attention should be paid to fabricating different types of biomolecule-based fractal nanomaterials. For the development of chiral nanoflowers, studies have mainly focused on developing CPL materials, chiral sensors, biocatalysts, and chiral plasmonic nanomaterials. The effects of nanoflowers on chiroptic-based device performance have been described in detail. Future work should seek new hybrid nanoflowers for the construction of CPL nanomaterials. Attributed to the abundant 'hot spots' generated by their specific surface geometry, nanoflowers are considered satisfactory SERS substrates. The enormous advantages of utilizing chiral nanoflowers for optical applications are included in the manuscript. Additionally, the combination of enzymes and nanoflowers offers an efficient strategy to develop biocatalysts with improved catalytic activity. We believe that diverse nanoflowers need to be investigated to broaden the application of nanoflowers for chiral amplification.

This review summarizes self-similar chiral nanomaterials synthesized using an individual-to-family approach. We hope self-extension of synthons will be accomplished in chiral communication, transmission, and amplification.

## Author contributions

Tingting Hong and Zhiqiang Cai were involved in project conceptualization, supervision, investigation, writing – original draft, writing – review and editing, as well as funding acquisition.

Wenhu Zhou and Songwen Tan were involved in resources and writing – original draft. Qi Zhou, Yilian Liu and Jiaqi Guan were involved in writing – original draft.

## Data availability

No primary research results, software or code have been included and no new data were generated or analysed as part of this review.

## Conflicts of interest

There are no conflicts to declare.

## Acknowledgements

For financial support of this work, we acknowledge the National Natural Science Foundation of China (81803495).

## References

- Q. Sallembien, L. Bouteiller, J. Crassous and M. Raynal, *Chem. Soc. Rev.*, 2022, **51**, 3436–3476.
- D. Avnir, *New Astron. Rev.*, 2021, **92**, 101596.
- B. H. Lee, N. A. Kotov and G. Arya, *ACS Nano*, 2021, **15**, 13547–13558.
- X. Deng, W. Li, Y. Wang and G. Ding, *TrAC, Trends Anal. Chem.*, 2020, **124**, 115804.
- Q. Wu, H. Lv and L. Zhao, *TrAC, Trends Anal. Chem.*, 2020, **129**, 115941.
- W. Fu, L. Tan and P. Wang, *ACS Nano*, 2023, **17**, 16326–16347.
- H. Zhang, S. Li, A. Qu, C. Hao, M. Sun, L. Xu, C. Xu and H. Kuang, *Chem. Sci.*, 2020, **11**, 12937–12954.
- X. Qiu, Y. Zhang, Y. Zhu, C. Long, L. Su, S. Liu and Z. Tang, *Adv. Mater.*, 2021, **11**, 2001731.
- J. Liu, L. Yang, P. Qin, S. Zhang, K. K. L. Yung and Z. Huang, *Adv. Mater.*, 2021, **16**, 2005506.
- Y. Y. Lee, R. M. Kim, S. W. Im, M. Balamurugan and K. T. Nam, *Nanoscale*, 2020, **12**, 58–66.
- N. H. Cho, A. Guerrero-Martínez, J. Ma, S. Bals, N. A. Kotov, L. M. Liz-Marzán and K. T. Nam, *Nat. Rev. Bioeng.*, 2023, 88–106.
- T. Hong, W. Zhou, S. Tan and Z. Cai, *Nanoscale Horiz.*, 2023, **8**, 1485–1508.
- H. Duan, Y. Li, Q. Li, P. Wang, X. Liu, L. Cheng, Y. Yu and L. Cao, *Angew. Chem., Int. Ed.*, 2020, **59**, 10101–10110.
- L. Ren, Y. Han, X. Hou, Y. Ni and J. Wu, *Chem*, 2021, **7**, 3442–3453.
- D. Chakraborty and P. S. Mukherjee, *Chem. Commun.*, 2022, **58**, 5558–5573.
- H. Wang, Y. Jin, N. Sun, W. Zhang and J. Jiang, *Chem. Soc. Rev.*, 2021, **50**, 8874–8886.
- D. Hu, J. Zhang and M. Liu, *Chem. Commun.*, 2022, **58**, 11333–11346.
- K. Su, W. Wang, S. Du, C. Ji, M. Zhou and D. Yuan, *J. Am. Chem. Soc.*, 2020, **142**, 18060–18072.
- Y. D. Yuan, J. Dong, J. Liu, D. Zhao, H. Wu, W. Zhou, H. X. Gan, Y. W. Tong, J. Jiang and D. Zhao, *Nat. Commun.*, 2020, **11**, 4927.
- Z. Wang, Q. P. Zhang, F. Guo, H. Ma, Z. H. Liang, C. H. Yi, C. Zhang and C. F. Chen, *Nat. Commun.*, 2024, **15**, 670.
- D. Zhang, T. K. Ronson, Y. Zou and J. R. Nitschke, *Nat. Rev. Chem.*, 2021, **5**, 168–182.
- J. Liu, Z. Wang, P. Cheng, M. J. Zaworotko, Y. Chen and Z. Zhang, *Nat. Rev. Chem.*, 2022, **6**, 339–356.
- E. Sánchez-González, M. Y. Tsang, J. Troyano, G. A. Craig and S. Furukawa, *Chem. Soc. Rev.*, 2022, **51**, 4876–4889.
- H. Wang, Y. Jin, N. Sun, W. Zhang and J. Jiang, *Chem. Soc. Rev.*, 2021, **50**, 8874–8886.
- G. Tikhomirov, P. Petersen and L. Qian, *Nature*, 2017, **552**, 67–71.
- T. Biesenthal, L. J. Maczewsky, Z. Yang, M. Kremer, M. Segev, A. Szameit and M. Heinrich, *Science*, 2022, **376**, 1114–1119.
- M. von Korf and T. Sander, *Sci. Rep.*, 2019, **9**, 967.
- S. Zheng, J. Han, X. Jin, Q. Ye, J. Zhou, P. Duan and M. Liu, *Angew. Chem., Int. Ed.*, 2021, **60**, 22711–22716.
- L. Zhang, M. Deng, Y. Duan, X. Wen, Y. Jiang, H. Jiang, Y. Ma and M. Liu, *Nano Res.*, 2022, **15**, 1079–1086.
- E. Azpeitia, G. Tichtinsky, M. L. Masson, A. Serrano-Mislata, J. Lucas, V. Gregis, C. Gimenez, N. Prunet, E. Farcot, M. M. Kater, D. Bradley, F. Madueño, C. Godin and F. Parcy, *Science*, 2021, **373**, 192–197.
- V. Shinde, M. Uthayakumar and R. Karthick, *Surf. Interfaces*, 2022, **32**, 102163.
- R. Liang, Y. Zhang, J. Zhang, Y. Gong, B. Huang, B. Wang, S. M. Xie and L. M. Yuan, *J. Chromatogr. A*, 2023, **1711**, 464444.
- K. Li, L. X. Xiong, Y. Wang, Y. P. Zhang, B. J. Wang, S. M. Xie, J. H. Zhang and L. M. Yuan, *J. Chromatogr. A*, 2022, **1679**, 463415.
- E. Martínez-Ahumada, D. He, V. Berryman, A. López-Olvera, M. Hernandez, V. Jancik, V. Martis, M. A. Vera, E. Lima, D. J. Parker, A. I. Cooper, I. A. Ibarra and M. Liu, *Angew. Chem., Int. Ed.*, 2021, **60**, 17556–17563.
- C. Dai, B. Gu, S. P. Tang, P. H. Deng and B. Liu, *Anal. Chim. Acta*, 2022, **1192**, 339376.
- S. Q. Gao, Y. T. Liu, L. H. Wang, Z. H. Wang, P. B. Liu, J. Gao and Y. J. Jiang, *ACS Catal.*, 2021, **11**, 5544–5553.
- Y. Wang, J. K. Chen, L. X. Xiong, B. J. Wang, S. M. Xie, J. H. Zhang and L. M. Yuan, *Anal. Chem.*, 2022, **94**, 4961–4969.
- X. Yang, Z. Ullah, J. F. Stoddart and C. T. Yavuz, *Chem. Rev.*, 2023, **123**, 4602–4634.
- D. Hu, J. Zhang and M. Liu, *Chem. Commun.*, 2022, **58**, 11333–11346.
- Y. Lu, H. Zhang, Y. Zhu, P. J. Marriott and H. Wang, *Adv. Funct. Mater.*, 2021, 2101335.
- Z. Sun, J. Hou, L. Li and Z. Tang, *Coord. Chem. Rev.*, 2020, **425**, 213481.

- 42 D. X. Cui, Y. Geng, J. N. Kou, G. G. Shan, C. Y. Sun, K. H. Zhang, X. L. Wang and Z. M. Su, *Nat. Commun.*, 2022, **13**, 4011.
- 43 P. Wagner, F. Rominger, W. S. Zhang, J. H. Gross, S. M. Elbert, R. R. Schröder and M. Mastalerz, *Angew. Chem.*, 2021, **133**, 8978–8986.
- 44 K. Acharyya and P. S. Mukherjee, *Angew. Chem.*, 2019, **131**, 8732–8745.
- 45 A. G. Slater, M. A. Little, A. Pulido, S. Y. Chong, D. Holden, L. Chen, C. Morgan, X. Wu, G. Cheng, R. Clowes, M. E. Briggs, T. Hasell, K. E. Jelfs, G. M. Day and A. I. Cooper, *Nat. Chem.*, 2017, **9**, 1–9.
- 46 X. L. Yang, Z. Y. Yang, R. Shao, R. F. Guan, S. L. Dong and M. H. Xie, *Adv. Mater.*, 2023, **35**, 2304046.
- 47 X. Niu, S. Yan, R. Zhao, H. Li, X. Liu and K. Wang, *ACS Appl. Mater. Interfaces*, 2023, **15**, 22435–22444.
- 48 M. Li, D. Yuan, B. Wu and M. Hong, *ACS Appl. Mater. Interfaces*, 2023, **15**, 22241–22250.
- 49 Z. Zheng, C. Yuan, M. Sun, J. Dong, Y. Liu and Y. Cui, *J. Am. Chem. Soc.*, 2023, **145**, 6100–6111.
- 50 Q. Dong, X. Guo, X. Qu, S. Bai, X. You, H. Cui, S. Qin and L. Gao, *Talanta*, 2023, **258**, 124415.
- 51 J. Y. Yue, L. P. Song, Y. H. Shi, L. Zhang, Z. X. Pan, P. Yang, Y. Ma and B. Tang, *Anal. Chem.*, 2023, **95**, 11078–11084.
- 52 T. He, R. Liu, S. Wang, I. K. W. On, Y. Wu, Y. Xing, W. Yuan, J. Guo and Y. Zhao, *J. Am. Chem. Soc.*, 2023, **145**, 18015–18021.
- 53 N. Xu, K. Su, E. M. El-Sayed, Z. Ju and D. Yuan, *Chem. Sci.*, 2022, **13**, 3582–3588.
- 54 Y. Wang, J. K. Chen, L. X. Xiong, B. J. Wang, S. M. Xie, J. H. Zhang and L. M. Yuan, *Anal. Chem.*, 2022, **94**, 4961–4969.
- 55 H. X. Li, T. P. Xie, K. Q. Yan, S. M. Xie, B. J. Wang, J. H. Zhang and L. M. Yuan, *Microchim. Acta*, 2020, **187**, 269.
- 56 T. Mitra, K. E. Jelfs, M. Schmidtman, A. Ahmed, S. Y. Chong, D. J. Adams and A. I. Cooper, *Nat. Chem.*, 2013, **5**, 276–281.
- 57 T. Hasell, M. A. Little, S. Y. Chong, M. Schmidtman, M. E. Briggs, V. Santolini, K. E. Jelfs and A. I. Cooper, *Nanoscale*, 2017, **9**, 6783–6790.
- 58 M. Pan, K. Wu, J. H. Zhang and C. Y. Su, *Coord. Chem. Rev.*, 2019, **378**, 333–349.
- 59 D. Zhang, T. K. Ronson, Y. Q. Zou and J. R. Nitschke, *Nat. Rev. Chem.*, 2021, **5**, 168–182.
- 60 C. Liu, J. Li, M. Lu, X. Jia, A. Yu and S. Zhang, *Sep. Purif. Technol.*, 2024, **332**, 125765.
- 61 E. Raee, B. Liu, Y. Yang, T. Namani, Y. Cui, N. Sahai, X. Li and T. Liu, *Nano Lett.*, 2022, **22**, 4421–4428.
- 62 K. Wu, K. Li, Y. J. Hou, M. Pan, L. Y. Zhang, L. Chen and C. Y. Su, *Nat. Commun.*, 2016, **7**, 10487.
- 63 Y. Li, J. Dong, W. Gong, X. Tang, Y. Liu, Y. Cui and Y. Liu, *J. Am. Chem. Soc.*, 2021, **143**, 20939–20951.
- 64 C. F. Liu, J. K. Chen, P. Guo, Y. R. Lu, Y. P. Yang, B. J. Wang, J. H. Zhang, S. M. Xie and L. M. Yuan, *Anal. Chim. Acta*, 2022, **1224**, 340197.
- 65 B. Tang, X. Zhang, L. Geng, L. Sun and A. Luo, *J. Chromatogr. A*, 2021, **1636**, 461792.
- 66 S. Chen, K. Li, F. Zhao, L. Zhang, M. Pan, Y. Z. Fan, J. Guo, J. Shi and C. Y. Su, *Nat. Commun.*, 2016, **7**, 13169.
- 67 A. Schmidt, A. Casini and F. E. Kühn, *Coord. Chem. Rev.*, 2014, **275**, 19–36.
- 68 J. Liu, T. Luo, Y. Xue, L. Mao, P. J. Stang and M. Wang, *Angew. Chem., Int. Ed.*, 2021, **60**, 5429–5435.
- 69 N. Ahmad, H. A. Younus, A. H. Chughtai and F. Verpoort, *Chem. Soc. Rev.*, 2015, **44**, 9–25.
- 70 Z. Li, Z. Mao, W. Zhou and Z. Chen, *Anal. Chim. Acta*, 2020, **1094**, 160–167.
- 71 S. Y. Zhang, C. X. Yang, W. Shi, X. P. Yan, P. Cheng, L. Wojtas and M. J. Zaworotko, *Chem*, 2017, **3**, 281–289.
- 72 J. Jiao, C. Tan, Z. Li, Y. Liu, X. Han and Y. Cui, *J. Am. Chem. Soc.*, 2018, **140**, 2251–2259.
- 73 E. M. El-Sayed, Y. D. Yuan, D. Zhao and D. Yuan, *Acc. Chem. Res.*, 2022, **55**, 1546–1560.
- 74 M. Pan, K. Wu, J. H. Zhang and C. Y. Su, *Coord. Chem. Rev.*, 2019, **378**, 333–349.
- 75 C. Zhu, H. Tang, K. Yang, Y. Fang, K. Y. Wang, Z. Xiao, X. Wu, Y. Li, J. A. Powell and H. C. Zhou, *J. Am. Chem. Soc.*, 2021, **143**, 12560–12566.
- 76 C. Zhu, K. Yang, H. Wang, Y. Fang, L. Feng, J. Zhang, Z. Xiao, X. Wu, Y. Li, Y. Fu, W. Zhang, K. Y. Wang and H. C. Zhou, *ACS Cent. Sci.*, 2022, **8**, 562–570.
- 77 G. H. Chen, Y. P. He, Y. Yu, H. Lv, S. Li, F. Wang, Z. G. Gu and J. Zhang, *Angew. Chem.*, 2023, **135**, e202300726.
- 78 Y. P. He, L. B. Yuan, J. S. Song, G. H. Chen, Q. Lin, C. Li, L. Zhang and J. Zhang, *Chem. Mater.*, 2018, **30**, 7769–7775.
- 79 G. H. Chen, Y. P. He, F. Wang, L. B. Yuan, H. Xu and J. Zhang, *Cryst. Growth Des.*, 2020, **20**, 6316–6320.
- 80 H. Jiang, W. Zhang, B. Hou, Y. Liu and Y. Cui, *CCS Chem.*, 2023, **5**, 1635–1643.
- 81 A. Yadav, P. Kulkarni, B. Praveenkumar, A. Steiner and R. Boomishankar, *Chem. – Eur. J.*, 2018, **24**, 14639–14643.
- 82 Z. G. Jiang, X. Wu, Z. X. Xu, C. H. Zhan and J. Zhang, *CrystEngComm*, 2020, **22**, 4206–4209.
- 83 K. Tanaka, T. Kawakita, M. Morawiak and Z. Urbanczyk-Lipkowska, *CrystEngComm*, 2019, **21**, 487–493.
- 84 G. F. S. Whitehead, S. J. Teat, K. J. Gagnon, G. A. Timco and R. E. P. Winpenny, *Chem. Commun.*, 2015, **51**, 3533–3536.
- 85 Z. Ju, G. Liu, Y. S. Chen, D. Yuan and B. Chen, *Chem. – Eur. J.*, 2017, **23**, 4774–4777.
- 86 W. Gong, D. Chu, H. Jiang, X. Chen, Y. Cui and Y. Liu, *Nat. Commun.*, 2019, **10**, 600.
- 87 X. L. Ma, Z. X. Wang, X. He, M. Shao and M. X. Li, *Inorg. Chem. Commun.*, 2018, **92**, 131–135.
- 88 G. Yuan, K. Z. Shao, X. L. Wang, Y. Q. Lan, D. Y. Du and Z. M. Su, *CrystEngComm*, 2010, **12**, 1147–1152.
- 89 B. T. Shahraki, S. Maghsoudi, Y. Fatahi, N. Rabiee, S. Bahadorikhalili, R. Dinarvand, M. Bagherzadeh and F. Verpoort, *Coord. Chem. Rev.*, 2020, **423**, 213484.
- 90 Q. H. Guo, Y. Jiao, Y. Feng and J. F. Stoddart, *CCS Chem.*, 2021, **3**, 1542–1572.
- 91 Y. Liu, M. O’Keeffe, M. M. J. Treacy and O. M. Yaghi, *Chem. Soc. Rev.*, 2018, **47**, 4642–4664.
- 92 G. Gil-Ramirez, D. A. Leigh and A. J. Stephens, *Angew. Chem., Int. Ed.*, 2015, **54**, 6110–6150.

- 93 Q. Wu, P. M. Rauscher, X. Lang, R. J. Wojtecki, J. J. de Pablo, M. J. A. Hore and S. J. Rowan, *Science*, 2017, **358**, 1434–1439.
- 94 C. Kulkarni, D. D. Nuzzo, E. W. Meijer and S. C. J. Meskers, *J. Phys. Chem. B*, 2017, **121**, 11520–11527.
- 95 S. De, B. Chi, T. Granier, T. Qi, V. Maurizot and I. Huc, *Nat. Chem.*, 2018, **10**, 51–57.
- 96 Q. Gan, X. Wang, B. Kauffmann, F. Rosu, Y. Ferrand and I. Huc, *Nat. Nanotechnol.*, 2017, **12**, 447–452.
- 97 M. D. Poli, W. Zawodny, O. Quinonero, M. Lorch, S. J. Webb and J. Clayden, *Science*, 2016, **352**, 575–580.
- 98 J. Zhang, D. Luo, C. Ma, L. Huang and Q. Gan, *Nat. Commun.*, 2021, **12**, 2659.
- 99 R. Zhu, I. Regeni, J. J. Holstein, B. Dittrich, M. Simon, S. Prévost, M. Gradzielski and G. H. Clever, *Angew. Chem., Int. Ed.*, 2018, **57**, 13652–13656.
- 100 Y. Lei, Q. Chen, P. Liu, L. Wang, H. Wang, B. Li, X. Lu, Z. Chen, Y. Pan, F. Huang and H. Li, *Angew. Chem.*, 2021, **133**, 4755–4761.
- 101 L. F. Ma, M. L. Han, J. H. Qin, L. Y. Wang and M. Du, *Inorg. Chem.*, 2012, **51**, 9431–9442.
- 102 H. Chen, D. Xiao, J. He, Z. Li, G. Zhang, D. Sun, R. Yuan, E. Wang and Q. L. Luo, *CrystEngComm*, 2011, **13**, 4988–5000.
- 103 A. Westcott, J. Fisher, L. P. Harding, P. Rizkallah and M. J. Hardie, *J. Am. Chem. Soc.*, 2008, **130**, 2950–2951.
- 104 D. Shaffer, J. Wang and L. H. Santos, *Nat. Commun.*, 2022, **13**, 7785.
- 105 J. Ying, Y. Xiao, J. Chen, Z. Y. Hu, G. Tian, G. Van Tendeloo, Y. Zhang, M. D. Symes, C. Janiak and X. Y. Yang, *Nano Lett.*, 2023, **23**, 7371–7378.
- 106 J. Fu, J. Jiao, H. Song, Z. Gu, Y. Liu, J. Geng, K. S. Jack, A. Du, J. Tang and C. Yu, *Chem. Mater.*, 2020, **32**, 341–347.
- 107 J. Li, J. Dai, S. Jiang, M. Xie, T. Zhai, L. Guo, S. Cao, S. Xing, Z. Qu, Y. Zhao, F. Wang, Y. Yang, L. Liu, X. Zuo, L. Wang, H. Yan and C. Fan, *Nat. Commun.*, 2020, **11**, 2185.
- 108 T. Kojima, K. Hirai, Y. Zhou, P. Weerappuli, S. Takayama and N. A. Kotov, *Langmuir*, 2016, **32**, 12468–12475.
- 109 A. Saha, J. Adamcik, S. Bolisetty, S. Handschin and R. Mezzenga, *Angew. Chem.*, 2015, **127**, 5498–5502.
- 110 F. L. Sendker, Y. K. Lo, T. Heimerl, S. Bohn, L. J. Persson, C. N. Mais, W. Sadowska, N. Paczia, E. Nußbaum, M. del Carmen Sánchez Olmos, K. Forchhammer, D. Schindler, T. J. Erb, J. L. P. Benesch, E. G. Marklund, G. Bange, J. M. Schuller and G. K. A. Hochberg, *Nature*, 2024, **628**, 894–900.
- 111 J. Shang, Y. Wang, M. Chen, J. Dai, X. Zhou, J. Kuttner, G. Hilt, X. Shao, J. Michael Gottfried and K. Wu, *Nat. Chem.*, 2015, **7**, 389–393.
- 112 L. Zhang, M. Deng, Y. Duan, X. Wen, Y. Jiang, H. Jiang, Y. Ma and M. Liu, *Nano Res.*, 2022, **15**, 1079–1086.
- 113 C. Zhou, X. Zhang, J. Ai, T. Ji, M. Nagai, Y. Duan, S. Che and L. Han, *Nano Res.*, 2022, **15**, 1295–1302.
- 114 D. Grober, I. Palaia, M. C. Uçar, E. Hannezo, A. Šarić and J. Palacci, *Nat. Phys.*, 2023, **19**, 1680–1688.
- 115 Z. Wang, Q. P. Zhang, F. Guo, H. Ma, Z. H. Liang, C. Yi, C. Zhang and C. F. Chen, *Nat. Commun.*, 2024, **15**, 670.
- 116 W. Jiang, Z. Qu, P. Kumar, D. Vecchio, Y. Wang, Y. Ma, J. H. Bahng, K. Bernardino, W. R. Gomes, F. M. Colombari, A. Lozada-Blanco, M. Veksler, E. Marino, A. Simon, C. Murray, S. R. Muniz, A. F. de Moura and N. A. Kotov, *Science*, 2020, **368**, 642–648.
- 117 J. N. B. D. Pelin, B. B. Gerbelli, B. M. Soares, A. M. Aguilar and W. A. Alves, *Catal. Sci. Technol.*, 2019, **9**, 4304–4313.
- 118 E. R. Silva, E. Listik, S. W. Han, W. A. Alvares, B. M. Soares, M. Rezad, J. Ruokolainen and I. W. Hamley, *Biophys. Chem.*, 2018, **233**, 1–12.
- 119 S. Roy, N. Javid, J. Sefcik, P. J. Halling and R. V. Ulijn, *Langmuir*, 2012, **28**, 16664–16670.
- 120 S. Naskar, A. Freytag, J. Deutsch, N. Wendt, P. Behrens, A. Kockritz and N. C. Bigall, *Chem. Mater.*, 2017, **29**, 9208–9217.
- 121 P. Sanpui, X. Zheng, J. C. Loeb, J. H. B. Jr, I. A. Khan, A. R. M. N. Afrooz, K. Liu, A. R. Badireddy, M. R. Wiesner, P. L. Ferguson, N. B. Saleh, J. A. Lednický and T. S. Attwood, *Part. Fibre Toxicol.*, 2014, **11**, 66.
- 122 I. A. Khan, N. Aich, A. R. M. N. Afrooz, J. R. V. Flora, P. A. Schierz, P. L. Ferguson, T. Sabo-Attwood and N. B. Saleh, *Chemosphere*, 2013, **93**, 1997–2003.
- 123 J. H. Bisesi Jr., J. Merten, K. Liu, A. N. Parks, A. R. M. N. Afrooz, J. B. Glenn, S. J. Klaine, A. S. Kane, N. B. Saleh, P. L. Ferguson and T. Sabo-Attwood, *Environ. Sci. Technol.*, 2014, **48**, 1973–1983.
- 124 H. Wang, L. Chen, Y. Feng and H. Chen, *Acc. Chem. Res.*, 2013, **46**, 1636–1646.
- 125 F. Carn, F. Boué, M. Djabourov, N. Steunou, T. Coradin, J. Livage, S. Floquet, E. Cadot and E. Buhler, *Soft Matter*, 2012, **8**, 2930–2944.
- 126 M. Uhlig, A. Fall, S. Wellert, M. Lehmann, S. Prévost, L. Wågberg, R. V. Klitzing and G. Nyström, *Langmuir*, 2016, **32**, 442–450.
- 127 W. T. Huang, M. C. Chang, C. Y. Chu, C. C. Chang, M. C. Li and D. M. Liu, *Carbohydr. Polym.*, 2019, **215**, 246–252.
- 128 C. C. Broomell, H. Birkedal, C. L. P. Oliveira, J. S. Pedersen, J. A. Gertenbach, M. Young and T. Douglas, *Soft Matter*, 2010, **6**, 3167–3171.
- 129 B. Zhao, H. Yu, K. Pan, Z. Tan and J. Deng, *ACS Nano*, 2020, **14**, 3208–3218.
- 130 Y. Duan, X. Liu, L. Han, S. Asahina, D. Xu, Y. Cao, Y. Yao and S. Che, *J. Am. Chem. Soc.*, 2014, **136**, 7193–7196.
- 131 S. Ponnada, D. B. Gorle, M. S. Kiai, S. Rajagopal, R. K. Sharma and A. Nowduri, *Mater. Adv.*, 2021, **2**, 5986–5996.
- 132 J. Hao, Y. Li, J. Miao, R. Liu, J. Li, H. Liu, Q. Wang, H. Liu, M. Delville, T. He, K. Wang, X. Zhu and J. Cheng, *ACS Nano*, 2020, **14**, 10346–10358.
- 133 Y. Zhou, T. Bai and Y. Duan, *Chem. Commun.*, 2023, **59**, 13207–13210.
- 134 F. Zhang, J. Ai, K. Ding, Y. Duan, L. Han and S. Che, *Chem. Commun.*, 2020, **56**, 4848–4851.
- 135 H. Savaloni, F. Haydari-Nasab and M. Malmir, *Appl. Surf. Sci.*, 2011, **257**, 9044–9055.
- 136 C. Zhou, S. Zhang, J. Ai, P. Li, Y. Zhao, B. Li, L. Han, Y. Duan and S. Che, *Chem. Mater.*, 2022, **34**, 53–62.

- 137 N. N. Zhang, H. R. Sun, Y. Xue, F. Peng and K. Liu, *J. Phys. Chem. C*, 2021, **125**, 10708–10715.
- 138 P. Huang, O. Pandoli, X. Wang, Z. Wang, Z. Li, C. Zhang, F. Chen, J. Lin, D. Cui and X. Chen, *Nano Res.*, 2012, **5**, 630–639.
- 139 Z. He, S. Zang, Y. Liu, Y. He and H. Lei, *Biosens. Bioelectron.*, 2015, **73**, 85–92.
- 140 H. Savaloni and R. Babaei, *Appl. Surf. Sci.*, 2013, **280**, 439–445.
- 141 S. Talu, M. Bramowicz, S. Kulesza, A. Ghaderi, S. Solaymani, H. Savaloni and R. Babaei, *J. Ind. Eng. Chem.*, 2016, **43**, 164–169.
- 142 B. Jia, C. Liu and X. Qi, *Fuel Process. Technol.*, 2020, **210**, 106578.
- 143 P. Cheng, M. Tang, Z. Chen, W. Liu, X. Jiang, X. Pei and W. Su, *React. Chem. Eng.*, 2020, **5**, 1973–1980.
- 144 G. Cao, J. Gao, L. Zhou, Y. He, J. Li and Y. Jiang, *ACS Appl. Nano Mater.*, 2018, **1**, 3417–3425.
- 145 M. Hao, G. Fan, Y. Zhang, Y. Xin and L. Zhang, *Int. J. Biol. Macromol.*, 2019, **126**, 539–548.
- 146 K. Li, J. Wang, Y. He, M. A. Abdulrazaq and Y. Yan, *J. Biotechnol.*, 2018, **281**, 87–98.
- 147 K. Bera, T. Ghosh and S. Basak, *J. Phys. Chem. C*, 2015, **119**, 1800–1808.
- 148 R. S. Bhosale, M. A. Kobaisi, S. V. Bhosale, S. Bhargava and S. V. Bhosale, *Sci. Rep.*, 2015, **5**, 14609.
- 149 J. Chen, Z. Guo, Y. Xin, Z. Gu, L. Zhang and X. Guo, *Coord. Chem. Rev.*, 2023, **489**, 215191.
- 150 Y. Li, H. Wu and Z. Su, *Coord. Chem. Rev.*, 2020, **416**, 213342.
- 151 X. Chen, L. Xu, A. Wang, H. Li, C. Wang, X. Pei, P. Zhang and S. G. Wu, *J. Chem. Technol. Biotechnol.*, 2019, **94**, 236–243.
- 152 X. Zhang, J. Xia, O. A. Tretiakov, M. Ezawa, G. Zhao, Y. Zhou, X. Liu and M. Mochizuki, *Nano Lett.*, 2023, **23**, 11793–11801.
- 153 Y. Sang, J. Han, T. Zhao, P. Duan and M. Liu, *Adv. Mater.*, 2019, 1900110.
- 154 A. Nitti and D. Pasini, *Adv. Mater.*, 2020, 1908021.
- 155 X. Y. Luo and M. Pan, *Coord. Chem. Rev.*, 2022, **468**, 214640.
- 156 J. Han, Y. Shi, X. Jin, X. Yang and P. Duan, *Chem. Sci.*, 2022, **13**, 6074–6080.
- 157 M. Zhang, Q. Guo, Z. Li, Y. Zhou, S. Zhao, Z. Tong, Y. Wang, G. Li, S. Jin, M. Zhu, T. Zhuang and S. H. Yu, *Sci. Adv.*, 2023, **9**, 9944.
- 158 Y. Dai, J. Chen, C. Zhao, L. Feng and X. Qu, *Angew. Chem.*, 2022, **61**, e202211822.
- 159 H. Chen, Z. G. Gu and J. Zhang, *J. Am. Chem. Soc.*, 2022, **144**, 7245–7252.
- 160 H. Yu, H. Huang, J. Liang and J. Deng, *Nanoscale*, 2018, **10**, 12163–12168.
- 161 L. Ji, Y. Zhao, M. Tao, H. Wang, D. Niu, G. Ouyang, A. Xia and M. Liu, *ACS Nano*, 2020, **14**, 2373–2384.
- 162 H. J. Wang, H. Y. Zhang, H. Wu, X. Y. Dai, P. Y. Li and Y. Liu, *Chem. Commun.*, 2019, **55**, 4499–4502.
- 163 J. Kwon, W. J. Choi, U. Jeong, W. Jung, I. Hwang, K. H. Park, S. G. Ko, S. M. Park, N. A. Kotov and J. Yeom, *Nano Convergence*, 2022, **9**, 32.
- 164 T. H. Xiao, Z. Cheng and K. Goda, *Small*, 2018, **14**, 1800485.
- 165 N. H. Cho, A. Guerrero-Martínez, J. Ma, S. Bals, N. A. Kotov, L. M. Liz-Marzán and K. T. Nam, *Nat. Rev. Bioeng.*, 2023, **1**, 88–106.
- 166 Y. Wen, M. Q. He, Y. L. Yu and J. H. Wang, *Adv. Colloid Interface Sci.*, 2021, **289**, 102376.
- 167 W. Ma, L. Xu, A. F. de Moura, X. Wu, H. Kuang, C. Xu and N. A. Kotov, *Chem. Rev.*, 2017, **117**, 8041–8093.
- 168 S. W. Im, H. Y. Ahn, R. M. Kim, N. H. Cho, H. Kim, Y. C. Lim, H. E. Lee and T. Nam, *Adv. Mater.*, 2020, **32**, 1905758.
- 169 N. H. Cho, G. H. Byun, Y. C. Lim, S. W. Im, H. Kim, H. E. Lee, H. Y. Ahn and K. T. Nam, *ACS Nano*, 2020, **14**, 3595–3602.
- 170 H. E. Lee, R. M. Kim, H. Y. Ahn, Y. Y. Lee, G. H. Byun, S. W. Im, J. Mun, J. Rho and K. T. Nam, *Nat. Commun.*, 2020, **11**, 263.
- 171 S. Li, Y. Liu, X. Tang, Z. Xu, L. Lin, Z. Xie, R. Huo, Z. A. Nan, Z. J. Guan, H. Shen and N. Zheng, *ACS Nano*, 2024, **18**, 13675–13682.
- 172 Y. Zheng, X. Li, L. Huang, X. Li, S. Yang, Q. Wang, J. Du, Y. Wang, W. Ding, B. Gao and H. Chen, *J. Am. Chem. Soc.*, 2024, **146**, 410–418.
- 173 M. Fan, G. F. S. Andrade and A. G. Brolo, *Anal. Chim. Acta*, 2020, **1097**, 1–29.
- 174 J. T. Garza and G. L. Cote, *Anal. Chem.*, 2017, **89**, 13120–13127.
- 175 H. Li, S. A. Haruna, W. Sheng, Q. Bei, W. Ahmad, M. Zareef, Q. Chen and Z. Ding, *TrAC, Trends Anal. Chem.*, 2023, **169**, 117365.
- 176 C. Zhou, Z. Miao, Y. Ren, Q. Fan, J. Han, X. Sun, H. Li, Y. Tu and R. Guo, *ACS Appl. Nano Mater.*, 2022, **5**, 9910–9919.
- 177 S. Wu, Q. Ye, D. Wu, Y. Tao and Y. Kong, *Anal. Chem.*, 2020, **92**, 11927–11934.
- 178 S. M. Wagalgave, S. D. Padghan, M. A. Kobaisi, D. D. La, K. Bhamidipati, N. Puvvada, R. S. Bhosale, S. V. Bhosale and S. V. Bhosale, *New J. Chem.*, 2020, **44**, 18092–18101.
- 179 Y. Yao, Q. Tang, S. Rosenfeldt, M. Krüsmann, M. Karg and K. Zhang, *Small*, 2021, **17**, 2102938.